



HAL
open science

HIV-1 Nef Hijacks Lck and Rac1 Endosomal Traffic To Dually Modulate Signaling-Mediated and Actin Cytoskeleton-Mediated T Cell Functions

Iratxe del Río-Iñiguez, Elena Vázquez-Chávez, Céline Cuche, Vincenzo Di Bartolo, Jérôme Bouchet, Andres Alcover

► **To cite this version:**

Iratxe del Río-Iñiguez, Elena Vázquez-Chávez, Céline Cuche, Vincenzo Di Bartolo, Jérôme Bouchet, et al.. HIV-1 Nef Hijacks Lck and Rac1 Endosomal Traffic To Dually Modulate Signaling-Mediated and Actin Cytoskeleton-Mediated T Cell Functions. *Journal of Immunology*, 2018, 201 (9), pp.2624 - 2640. 10.4049/jimmunol.1800372 . pasteur-01907920

HAL Id: pasteur-01907920

<https://pasteur.hal.science/pasteur-01907920v1>

Submitted on 29 Oct 2018

HAL is a multi-disciplinary open access archive for the deposit and dissemination of scientific research documents, whether they are published or not. The documents may come from teaching and research institutions in France or abroad, or from public or private research centers.

L'archive ouverte pluridisciplinaire **HAL**, est destinée au dépôt et à la diffusion de documents scientifiques de niveau recherche, publiés ou non, émanant des établissements d'enseignement et de recherche français ou étrangers, des laboratoires publics ou privés.

1 **Accepted manuscript without last corrections:**

2 **Reference of the article published**

3 Del Río-Iñiguez, I., Vázquez-Chávez, E., Cucho, C., Di Bartolo, V., Bouchet, J. and Alcover,
4 A. 2018. HIV-1 Nef Hijacks Lck and Rac1 Endosomal Traffic To Dually Modulate
5 Signaling-Mediated and Actin Cytoskeleton-Mediated T Cell Functions. Journal of
6 Immunology, 201(9):2624-2640. doi: 10.4049/jimmunol.1800372.

6

7

8 **HIV-1 Nef hijacks Lck and Rac1 endosomal traffic to dually modulate signaling- and**
9 **actin cytoskeleton-mediated T cell functions.**

10

11 Iratxe del Río-Iñiguez^{*,†,§}, Elena Vázquez-Chávez^{*,†}, Céline Cucho^{*,†}, Vincenzo Di Bartolo^{*,†},
12 Jérôme Bouchet^{*,†,1,2} and Andrés Alcover^{*,†,2}

13

14 ^{*}Institut Pasteur, Department of Immunology, Lymphocyte Cell Biology Unit, Paris. France.

15 [†]INSERM U1221. Paris France.

16 [§]Sorbonne Université, Collège Doctoral, Paris, France

17

18 **Running title:** Nef hijacks T cell signaling and cytoskeletal regulators

19

20 **Correspondence:**

21 Andrés Alcover PhD. Institut Pasteur, Unité de Biologie Cellulaire des Lymphocytes. 28, Rue
22 Dr Roux. 75724 Paris Cedex 15. France. Tel: office +33 1 40 61 30 64 // cellular: +33 6 84 47
23 22 30. Email: andres.alcover@pasteur.fr

24 Jérôme Bouchet, PhD. Institut Cochin INSERM, U1016, CNRS, UMR8104, Université Paris
25 Descartes, Sorbonne Paris Cité, Paris, France. Email: jerome.bouchet@inserm.fr

26

27

28

29 **Abstract**

30 Endosomal traffic of TCR and signaling molecules regulates immunological synapse
31 formation and T cell activation. We recently showed that Rab11 endosomes regulate the
32 subcellular localization of the tyrosine kinase Lck and of the GTPase Rac1 and control their
33 functions in TCR signaling and actin cytoskeleton remodeling. HIV-1 infection of T cells
34 alters their endosomal traffic, activation capacity and actin cytoskeleton organization. The
35 viral protein Nef is pivotal for these modifications. We hypothesized that HIV-1 Nef could
36 jointly alter Lck and Rac1 endosomal traffic and concomitantly modulate their functions.
37 Here, we show that HIV-1 infection of human T cells sequesters both Lck and Rac1 in a
38 pericentrosomal compartment in a Nef-dependent manner. Strikingly, the Nef-induced Lck
39 compartment contains signaling competent forms (phosphorylated on key Tyr residues) of
40 Lck and some of its downstream effectors, TCR ζ , ZAP70, SLP76 and Vav1, avoiding the
41 proximal LAT adaptor. Importantly, Nef-induced concentration of signaling molecules was
42 concomitant with the upregulation of several early and late T cell activation genes. Moreover,
43 preventing the concentration of the Nef-induced Lck compartment, by depleting the Rab11
44 effector FIP3, counteracted Nef-induced gene expression upregulation. In addition, Nef
45 extensively sequesters Rac1 and down regulates Rac1-dependent actin cytoskeleton
46 remodeling, thus reducing T cell spreading. Therefore, by modifying their endosomal traffic,
47 Nef hijacks signaling and actin cytoskeleton regulators to dually modulate their functional
48 outputs. Our data shed new light into the molecular mechanisms that modify T cell
49 physiology during HIV-1 infection.

50

51 **Introduction**

52 Antigen recognition triggers T cell polarization towards the antigen presenting cell
53 (APC). This process involves the reorganization of the actin and microtubule cytoskeleton,
54 the reorientation of intracellular vesicle traffic and the generation of dynamic signaling and
55 adhesion complexes at the T cell-APC contact site, termed the immunological synapse.
56 Altogether, these processes control immunological synapse formation and function, ensuring
57 T cell activation leading to T cell proliferation and differentiation, and T cell effector
58 functions, like polarized secretion of cytokines and cytotoxic granules (1, 2).

59 TCR signal transduction involves the CD3 γ , δ , ϵ and ζ subunits, which contain in their
60 intracellular regions immune-receptor tyrosine-based activation motifs (ITAM) that are
61 phosphorylated soon after TCR engagement. ITAM phosphorylation by the Src family protein
62 tyrosine kinase Lck facilitates the recruitment of downstream effectors, including the tyrosine
63 kinase ZAP70 (zeta-associated protein of 70 kDa), which is recruited to phosphorylated
64 ITAMs of TCR ζ *via* its SH2 domains. This induces ZAP70 tyrosine phosphorylation and
65 activation, the subsequent tyrosine phosphorylation of the signaling adaptors LAT and SLP76
66 and the recruitment of effectors to these adaptors. Altogether, these proteins form a
67 signalosome necessary to proceed to downstream activation events, including the activation
68 of phospholipase C (PLC)- γ 1, the generation of lipid second messengers, calcium flux, and
69 the activation of serine-threonine kinases, like MAP and protein kinase C (PKC) kinases. The
70 coordinated action of these different signaling molecules drives the activation of transcription
71 factors (e. g. NFAT, NF κ B and AP1), which in turn activate the expression of genes involved
72 in T cell growth, differentiation and the production of cytokines, crucial for the development
73 of adaptive immune responses (3, 4).

74 HIV-1 infects CD4⁺ T cells, subverting a variety of T cell physiological mechanisms.
75 This facilitates the production of viral particles and their transmission to other cells eventually
76 leading to chronic viral infection, while reducing the impact of the host immune defenses.
77 HIV-1 genome encodes several “accessory” proteins that are key for the HIV-1 subversion of
78 infected cell processes. Among them, Nef is crucial for *in vivo* viral replication, and AIDS
79 pathogenesis. Nef is abundantly expressed early after infection and optimizes the intracellular
80 environment to improve virus replication and reduce host immunity by modulating endosomal
81 traffic, actin cytoskeleton components and cell activation in infected T cells. As a
82 consequence, HIV-1 infection modifies the expression of several T cell surface molecules,
83 including CD4, CD28, MHC I and II (5), it alters cytoskeleton remodeling and its associated

84 cellular events (6-14), and it modulates T cell activation by affecting various signaling
85 pathways (15, 16). HIV-1 Nef interferes with Lck and LAT endosomal traffic to the
86 immunological synapse, altering T cell activation (17-19). The action of Nef on these
87 processes occurs through the presence of specific motifs in its primary sequence, allowing
88 interactions with a number of cellular proteins. Nef may also modify some intracellular traffic
89 pathways, resulting in the modulation of processes regulated by proteins transported through
90 those pathways.

91 We and others have shown that the TCR and the signaling molecules Lck and LAT are
92 associated with distinct endosomal and Golgi intracellular compartments. Their traffic to the
93 immunological synapse is differentially regulated and is crucial for TCR signal transduction
94 (20-30). Interestingly, we also observed that the GTPase Rac1, a key actin cytoskeleton
95 regulator, is also associated with recycling endosomes that control Rac1 subcellular
96 localization, its targeting to the immunological synapse and its ability to regulate actin
97 remodeling in T cells (31, 32).

98 Here, we performed a systematic analysis of the potential interplay between HIV-1 Nef
99 and the T cell activation molecular machinery, by analyzing its capacity to control the
100 subcellular localization and activation of signaling molecules downstream of the TCR, and its
101 consequence for T cell physiology. Our results show that Nef exerts a refined control of
102 signaling and cytoskeleton regulators to modulate T cell activation and cytoskeleton mediated
103 events.

104

105 **Materials and Methods**

106 *Expression vectors, small interfering RNA, viruses, primers and antibodies*

107 Vectors encoding green fluorescent protein (GFP), WT and mutant GFP-tagged HIV-1
108 NL4-3 Nef (Nef-GFP and Nef PXXP/AXXA-GFP) were previously described (33, 34). Wild
109 type and Nef-deleted (NL4-3-based) proviral plasmids (HIV-1 WT and HIV-1 Δ Nef,
110 respectively) have already been described (35, 36). pCMV-VSV-G was a gift from R.
111 Weinberg (Addgene plasmid # 8454) (37).

112 FIP3 was depleted with siRNA duplexes based on human FIP3 sequence described
113 elsewhere: siFIP3.1 (5'-AAGGGATCACAGCCATCAGAA-3') and siFIP3.2 (5'-
114 AAGGCAGTGAGGCGGAGCTGTT-3') (28, 31).

115 Virions were produced by the transient calcium-phosphate DNA precipitation
116 technique. HEK293T cells were transfected with 20 μ g proviral DNA. 72 h later supernatant
117 was recovered, centrifuged and cell free virion stocks were stored at -80°C. The concentration
118 of p24 antigen in viral stocks was measured by a quantitative enzyme-linked immunosorbent
119 assay (Perkin Elmer).

120 Antibodies and primer sequences are described in detail in the Supplemental Tables 1-3.

121 *Cells, cell culture, infection and transfection assays*

122 Human peripheral blood T cells from healthy volunteers were obtained from the French
123 National Blood Bank (Etablissement Français du Sang, EFS) and through the ICAReB core
124 facility at the Institut Pasteur (NSF96-900 certified, from sampling to distribution, reference
125 BB-0033-00062/ICAReB platform/ Institut Pasteur, Paris, France/BBMRI AO203/ 1
126 distribution/access: 2016, May 19th, [BIORESOURCE]), under the CoSIImmGen protocol
127 approved by the Committee of Protection of Persons, Ile de France-1 (no. 2010-dec-12483).
128 Informed consent was obtained from all subjects. Peripheral blood mononuclear cells
129 (PBMCs) were isolated by centrifugation through Ficoll-Hypaque from healthy donors.
130 PBMCs were cultured in RPMI 1640 medium containing 10% foetal calf serum (FCS), 1 mM
131 sodium pyruvate and 1% Penicillin-Streptomycin. For HIV-1 infection assays, PBMCs were
132 cultured with 5 μ g/mL PHA for two days, then infected with the equivalent of 2 μ g/mL of
133 capsid protein of 24 kDa (p24) of either WT or Δ Nef HIV-1 virions during 16 h. Cells were
134 then washed and resuspended in RPMI 1640 medium supplemented with 10% FCS and
135 10U/mL IL-2 for 3 days, before been used for immunofluorescence assays.

136 For transfection assays of primary cells, CD4⁺ T cells were further purified using the
137 CD4⁺ T cell isolation kit (Miltenyi Biotech) and cultured in RPMI 1640 medium containing

138 10% FCS, 1 mM sodium pyruvate, and nonessential amino acids. Isolated CD4⁺ T cells were
139 transfected with 10 µg plasmid DNA using the Amaxa Nucleofector system and the Human T
140 Cell Nucleofector kit (Lonza). Cells were harvested and used for immunofluorescence
141 analysis 24 h after transfection.

142 The human T cell line Jurkat clone J77cl20 was previously described (17). Jurkat were
143 cultured in RPMI 1640 containing 10% FCS. For HIV-1 infection assays, 5x10⁶ Jurkat cells
144 were infected with 2 µg of cell free HIV-1 virions or VSV-pseudotyped virions during 16 h.
145 Cells are then washed and resuspended in RPMI 1640 medium supplemented with 10% FCS
146 for 3 days (or 36 h for the VSV-pseudotyped virions), before being harvested.

147 For siRNA, a total of 2 nmol of control or FIP3 siRNA were used per 10⁷ Jurkat cells. 2
148 transfections were performed at 24 h interval with a Neon Transfection system (Life
149 Technologies), using the following protocol: 1400 V, 10 ms, 3 pulses. 72 h after the first
150 transfection cells were harvested and processed for analysis. In the case of plasmid
151 transfection, the Neon Transfection system was used in the same conditions to electroporate
152 10⁷ Jurkat cells with 10 µg plasmid DNA. Cells were harvested and processed for analysis 24
153 h after the transfection. When both infection and FIP3 depletion conditions were applied,
154 Jurkat cells were previously transfected with siRNA, and consecutively infected with VSV-
155 pseudotyped virions for 36 h, with a total of 72 h from the first transfection, before the cells
156 were harvested and processed for analysis.

157 ***Immunofluorescence***

158 Immunofluorescence and confocal imaging was performed as previously described (38,
159 39). Coverslips were coated with poly-L-lysine 0.002 % (w/v) in water (Sigma-Aldrich).
160 Cells were plated onto the coverslips for 3 min (if not otherwise indicated), then fixed with 4
161 % paraformaldehyde for 20 min at room temperature (RT), washed in phosphate buffer saline
162 (PBS), and incubated 30 min in PBS, 1 % bovine serum albumin (wt/vol) (PBS-BSA) to
163 prevent unspecific binding. Coverslips were then incubated 1 h at RT in PBS-BSA with 0.1 %
164 Triton X-100 and the indicated dilution of primary antibody. Coverslips were rinsed 3 times
165 in PBS-BSA and then incubated with the corresponding fluorescent-coupled secondary
166 antibody for 1 h at RT. After 3 washes in PBS-BSA, coverslips were mounted on microscope
167 slides using 8 µl of ProLongGold Antifade mounting medium with DAPI (Life
168 Technologies).

169 ***Confocal microscopy, image post-treatment and analysis***

170 Confocal images were acquired with a LSM 700 confocal microscope (Carl Zeiss) using
171 the Plan-Apochromat 63x objective. Optical confocal sections were acquired using ZEN
172 software (Carl Zeiss) by intercalating green and red laser excitation to minimize channel cross
173 talk. Confocal optical sections were acquired at 0.2 μm depth intervals and images were
174 treated by deconvolution with the Huygens Pro Software (version 14.10, Scientific Volume
175 Imaging). A 2D visualization of 3 consecutive confocal sections (cut of 0.4 μm depth,)
176 centered on the Nef induced endosomal compartment, when visible, or on a mid-section of
177 the cell, was generated from a sum intensity projection using Fiji software (40). Images
178 showing the density gradient fluorescent intensities were obtained with the mpl-Inferno LUT
179 of Fiji software.

180 Colocalization analyses were performed on the whole compartment (Nef, Lck or Rac1)
181 of deconvoluted images using Fiji software and the JACoP plugin (41). Threshold was
182 automatically determined using the Costes method autothreshold determination (42). Analysis
183 plots show the Pearson Correlation Coefficient. Colocalization scatter plot images show one
184 representative colocalization analysis of the whole analysis and were obtained using the
185 Colocalization Threshold plugin of the Fiji software. Statistical analyses were carried out
186 using the nonparametrical Mann-Whitney test of Prism software (Graphpad).

187 Images to quantify phospho-protein accumulation in the Lck compartment were
188 acquired at 1 μm depth intervals in the z-axis to avoid fluorescence overlap. Fluorescence
189 intensity in the area corresponding to the Lck compartment was calculated in percentage of
190 the total fluorescence of the cell. Statistical analyses were carried out using the
191 nonparametrical Mann-Whitney test of Prism software (Graphpad).

192 For densitometry profile analysis, a z-stack of 1 μm confocal optical sections was
193 acquired for each cell. Fluorescence intensity of pY319-ZAP70 or Rac1 was measured across
194 cells, including plasma membrane and the Nef pericentrosomal compartment.

195 *Analysis of cell spreading*

196 Cells were plated on poly-L-lysine coated coverslips, incubated at RT for the indicated
197 times and fixed with 4 % paraformaldehyde for 20 min. Coverslips were then treated as
198 previously described in the immunofluorescence section above, using a phalloidin labeled
199 antibody to stain F-actin. For the measurement of cell spreading, z-stacks of 0.5 μm confocal
200 optical sections were acquired. Two contiguous sections starting from the coverslip surface
201 were stacked, and cell surface was measured on the phalloidin staining using the Fiji Analyse

202 Particles tool, on GFP positive particles larger than 20 μm^2 . Statistical analyses were carried
203 out using the nonparametrical Mann-Whitney test of Prism software (Graphpad).

204

205 *Activation analysis*

206 Cells were stimulated by incubation with 10 $\mu\text{g}/\text{mL}$ of soluble CD3 mouse antibody
207 (UCHT1) and 10 $\mu\text{g}/\text{mL}$ of CD28 at 37°C. At the indicated times, cells were plated on poly-
208 L-lysine coated coverslips as previously described, fixed with 4 % paraformaldehyde for 20
209 min at RT, washed in PBS and incubated 30 min in PBS-BSA before immunofluorescence
210 was performed.

211 *Flow cytometry*

212 Infection levels were analyzed by flow cytometry using a MACSQuant Analyzer
213 (Miltenyi biotech). Cells were isolated, fixed with 4 % paraformaldehyde for 20 min at RT,
214 washed in PBS, and incubated with the appropriate dilution of fluorescent-labeled antibody in
215 PBS-BSA. For fluorescence intensity levels of intracellular phospho-proteins, fixed cells were
216 incubated in PBS-BSA with 0.1 % Triton X-100 and the indicated dilution of primary
217 antibody and secondary fluorescent-labeled antibody. Flow cytometry data were analyzed
218 with FlowJo software (FlowJo, LLC), restricting the analyses to single-cells using FSC-H/W
219 signals.

220 *Western blot*

221 Cells were lysed for 30 min in ice-cold buffer composed of 150 mM NaCl, 20 mM Tris
222 pH 7.4, 0.25 % lauryl- β -maltoside, 4 mM orthovanadate, 1 mM EGTA, 50 mM NaF, 10 mM
223 $\text{Na}_4\text{P}_2\text{O}_7$, 1mM MgCl_2 and protease inhibitors (1mM AEBSF, 10 $\mu\text{g}/\text{mL}$ Aprotinin, 10 $\mu\text{g}/\text{mL}$
224 Leupeptin). Cells lysates were centrifuged at 20,800 xg for 10 min at 4°C. Equal amount of
225 protein extract was loaded in NuPAGE 4-12% Bis-Tris gels (Life Technologies) by using the
226 BCA assay Kit (Thermo Fisher Scientific). Protein transfer to nitrocellulose blots (LI-COR
227 Biosciences) was performed using the BIO-RAD system and a transfer buffer composed of 25
228 mM Tris, 1,92 mM Glycine, 20 % EtOH, 0.1 % SDS. Membranes were saturated with
229 blocking buffer (Rockland Immunochemicals) and incubated with primary antibodies for 1 h
230 at RT or overnight at 4°C in blocking buffer. After incubation with secondary antibodies, an
231 Odyssey scanner (LI-COR Biosciences) was used to detect and imaged near-infrared
232 fluorescence. Images of blots were quantified using Fiji software.

233 ***mRNA measurements by RT-qPCR***

234 Total RNA was extracted using the RNeasy Mini Plus Kit (Qiagen), following the
235 manufacturer's instructions. cDNA was prepared from 1 µg of total RNA using iScript cDNA
236 synthesis kit (BIO-RAD). Gene products were quantified by qPCR using the FastStart
237 Universal SYBR Green PCR master mix (Roche) and the ABI PRISM 7900HT technology.
238 Most of the cases, qPCR quantifications were performed at least in 3 replicates and its
239 quantity values were calculated by the Relative Standard Curve Method and normalized to the
240 mRNA expression of the *B2M* housekeeping gene.

241 Primer sequences used to target the different genes are described in Supplemental
242 Table-3.

243 ***Statistics***

244 Statistical analyses were carried out using Prism software (Graphpad V.7). Details
245 about the data presentation, the experimental replication, and the adequate statistical tests
246 used are included in the individual Fig. legends. Data met the assumptions of the statistical
247 tests and its distribution was previously checked using the Shapiro-Wilk normality test.
248 Horizontal bars in plots represent the mean ± SEM. p values are represented as follow: ****,
249 p<0.0001; ***, p<0.001; **, p<0.01; *, p<0.05; non-significant (ns), p ≥0.05.

250

251 **Results**

252 **HIV-1 sequesters Lck and Rac1 in intracellular compartments in a Nef-dependent**
253 **manner.**

254 We and others have shown that HIV-1 Nef subverts the intracellular traffic of Lck and
255 its function as a TCR signaling molecule at the immunological synapse (17-19, 43). The
256 molecular mechanism involved in Lck retention by Nef is not completely elucidated, and may
257 involve, at least in part, the Lck traffic regulatory protein Unc119 and the transferrin recycling
258 endosomal compartment (17, 19, 34) that are regulated by the Rab11 GTPase (22, 44).

259 We have recently shown that Lck is associated with the Rab11⁺ endosomal
260 compartment and its function in TCR signaling is regulated by the Rab11 effector FIP3
261 (Rab11 family interacting protein-3) (28). Interestingly, T cells overexpressing FIP3 retain
262 Lck in their Rab11⁺ endosomal compartment, in a similar manner than Nef (17, 28).
263 Moreover, we have shown that Rac1 is also associated with Rab11⁺ endosomes and its

264 subcellular localization and function are regulated by FIP3 (31). These findings prompted us
265 to hypothesize that Nef could jointly alter Lck and Rac1 endosomal traffic, modulating their
266 functions concomitantly. Therefore, we analyzed the intracellular localization of Lck and
267 Rac1 upon HIV-1 infection by wild type (WT) and Nef-deficient (Δ Nef) viruses, as well as in
268 T cells expressing a Nef-GFP chimeric protein.

269 We indeed observed that HIV-1 infection in both primary and Jurkat T cells induced the
270 accumulation of Lck and Rac1, in a Nef-dependent manner. Lck and Rac1 concentrate in the
271 pericentrosomal area, while partially disappear from their cortical localization (Fig. 1A-1D).
272 Moreover, expression of Nef alone was sufficient for the intracellular relocation of both
273 Lck and Rac1 (Fig. 2A, 2C). Both molecules colocalized with Nef, although the overlap of
274 Rac1 and Nef was more extensive than that of Nef and Lck (Fig. 2A-2C, 8A). The Nef-
275 induced Lck compartment colocalized with Rab11 and not with TGN46, indicating that Lck is
276 mainly located in recycling endosomes (Fig. 2D, 2E).

277 Hence, HIV-1 Nef is necessary and sufficient to induce the concomitant intracellular
278 relocation of Lck and Rac1 in intracellular compartments, prompting us to investigate the
279 characteristics and functional consequences of these compartments.

280

281 **Nef-induced Lck endosomal compartment concentrates active Lck together with**
282 **signaling competent TCR ζ , ZAP70, SLP76 and Vav1.**

283 Lck kinase activity is regulated by the balanced phosphorylation of two tyrosine
284 residues, Tyr394, which favors kinase activity and substrate interaction, and Tyr505, which
285 prevents it, by stabilizing Lck in a folded conformation. The two species are present at
286 equilibrium in resting T cells and their phosphorylation ratio does not change upon TCR
287 engagement (45). This suggests that TCR signal transduction may be triggered by changes in
288 localization of active forms of Lck that facilitate Lck contiguity to its substrates (e. g. delivery
289 of endosomes carrying Lck to the immunological synapse). In this line, we have recently
290 shown that modifying the endosomal localization of Lck changes the activation capacity of T
291 cells, as assessed by the phosphorylation status of Lck and ZAP70 substrates (28).

292 To investigate the potential functional effects of Nef-induced endosomal accumulation
293 of Lck, we analyzed whether active forms of Lck were present in that compartment and if so,
294 whether there was an effect on Lck substrates and downstream effectors. To this end, we
295 performed a systematic analysis in Jurkat T cells expressing GFP-tagged Nef protein. This

296 experimental set up provides sufficient spatial resolution to analyze these vesicular
297 compartments, while eliminating the influence of other viral proteins. The use of specific
298 antibodies directed to phosphorylated tyrosine (pTyr) residues allowed us to distinguish
299 whether signaling molecules were in their signaling-competent phosphorylated state (e.g.
300 pTyr residues described to interact with other signaling molecules).

301 We observed that active phosphorylated Lck (pTyr394) concentrates in the Nef-induced
302 Lck compartment (Fig. 2B). Moreover, the phosphorylated forms of TCR ζ (pTyr142) and
303 ZAP70 (pTyr319), both substrates of Lck and interacting with each other upon TCR ζ
304 phosphorylation, are enriched within the Lck endosomal compartment, in which significantly
305 colocalize with Lck (Fig. 3A, 3B, 4A). Interestingly, the signaling adaptors LAT and SLP76
306 that interact with each other upon LAT phosphorylation by ZAP70 (3), are differentially
307 concentrated at the Nef-induced Lck compartment: pLAT (pTyr191) is neither concentrated
308 nor colocalized with Lck, while pSLP76 (pTyr128) accumulates and colocalizes with Lck, but
309 to a lesser extent than pTCR ζ and pZAP70 (Fig. 3C, 3D, 4A). Therefore, these findings show
310 that Nef sequesters the “initial triggering complex” formed by Lck, TCR ζ and ZAP70,
311 apparently separating the two components of the “signal amplification complex” formed by
312 the phosphorylated adaptors LAT and SLP76 (3, 4).

313 Importantly, concentration of phosphorylated Lck substrates in the pericentrosomal
314 compartment was related with Lck accumulation, since overexpression of the Nef
315 P₇₂XXP₇₅/AXXA mutant, which does not induce Lck accumulation (46), does not result in
316 pZAP70 accumulation (Fig. 4B, 4C). Moreover, the capacity of Nef to increase total pZAP70,
317 as assessed by flow cytometry, was significantly reduced in cells expressing the Nef
318 P₇₂XXP₇₅/AXXA mutant (Fig. 4D).

319 In addition, we found phosphorylated Vav1 (pTyr174) significantly concentrated at the
320 Nef-induced Lck endosomal compartment colocalizing with Lck (Fig. 3E, 4A). Vav1 is
321 involved in both the TCR-CD3 and CD28 signaling pathways acting as signaling adaptor
322 molecule (47, 48). Moreover, Vav1 is associated with the CD28 intracellular region *via* the
323 signaling adaptor Grb2 (48). CD28 is downregulated during HIV-1 infection in a Nef- and
324 Vpu-dependent manner, inducing CD28 internalization and degradation (5, 49, 50). In
325 agreement with this, we observed that Nef expression induces the accumulation of CD28 in a
326 pericentrosomal compartment that co-localizes with Nef (Fig. 5 A, B). However, we did not
327 find significant co-localization between CD28 and pVav1 in this compartment (Fig. 5C, 5D).
328 In contrast, we observed significant co-localization between intracellularly accumulated

329 CD28 and Rac1 (Fig. 5E, 5F). This is consistent with the extensive colocalization in the
330 pericentrosomal compartment of Nef and CD28 and of Nef and Rac1). Therefore, Nef-
331 induced pVav1 accumulation in the Nef-induced Lck compartment seems not to be the
332 consequence of recruitment of CD28-associated Vav1, but of a possible soluble fraction.
333 Finally, Vav1 is a regulator (guanine exchange factor, GEF) of Rac1, controlling its activity
334 on actin cytoskeleton dynamics (51). Its accumulation in the Nef-induced Lck compartment
335 under its GEF active form (pTyr174) could be relevant, at least in part for the Nef influence
336 on Rac1 activity.

337 Altogether, these data show that Nef expression induces the concentration of activation-
338 competent signaling molecules belonging to the TCR signaling pathways, leaving other
339 molecules unperturbed.

340

341

342 **Nef does not induce the relocalization of signaling effectors downstream of Lck, TCR ζ ,** 343 **ZAP70 and Vav1**

344 We next investigated whether the subcellular localization of signaling proteins
345 downstream of Lck, ZAP70, Vav1 and Rac1 was modified in Nef-expressing cells. To this
346 end, we analyzed the intracellular localization of a number of signaling molecules of the
347 TCR-CD28 signaling pathways leading to the activation of NFAT, NF κ B and AP1 (Fos and
348 Jun) transcription factors that together drive T cell differentiation, cytokine production and
349 eventually T cell proliferation (1). Among these downstream signaling proteins, PLC γ 1 is
350 activated through Lck and ZAP70-mediated tyrosine phosphorylation to give rise to two key
351 phospholipids second messengers, inositol trisphosphate (IP3) and diacylglycerol (DAG). IP3
352 regulates calcium flux from the endoplasmic reticulum, while DAG activates protein kinase C
353 (PKC) serine threonine kinases. Increase in intracellular calcium concentration then activates
354 the serine phosphatase calcineurin that dephosphorylates NFAT transcription factor, inducing
355 its translocation to the nucleus. In turn, PKC θ may phosphorylate and activate the kinase
356 Ikk β , inducing the NF κ B signaling pathway and NF κ B nuclear translocation. Moreover,
357 binding of Grb2-SOS to phosphorylated LAT facilitates Ras activation and the triggering of
358 the MAP kinase cascade involving Raf, MEK, Erk1/2 and Elk serine/threonine kinases that
359 activate the Fos transcription factor. Finally, Vav1 cooperates with PI3K in the CD28

360 cosignaling pathway to activate the GTPase Rac1 that in turn activates the Jun kinase (JNK)
361 and the Jun transcription factor (1).

362 Therefore, we analyzed the effect of Nef-GFP expression in the subcellular localization
363 of proteins and active forms of a number of these key signaling molecules, including Fyn,
364 AKT, pPLC γ 1, NEMO, BCL10, CARMA1, mTOR, NF- κ B (p105 and p65 subunits), PI3K,
365 PKC θ , pT538-PKC θ , PKC ζ , pThr202pY204-Erk1/2, pY185-JNK. We did not find any of
366 these proteins relocalized to the Nef-induced Lck endosomal compartment (Supplementary
367 Fig. S1A-S1D).

368 These data indicate that Nef effects on the localization of T cell signaling molecules
369 mainly concerns the TCR initiation signaling complex, but does not affect downstream
370 signaling molecules.

371

372

373 **Nef-induced accumulation of Lck in the endosomal compartment is concomitant with**
374 **differential modulation of T cell activation pathways.**

375 The accumulation of signaling competent forms of Lck, TCR ζ , ZAP70 and Vav1
376 suggests that HIV-1 infection may generate *via* Nef an autonomous “endosomal signaling
377 compartment” that delivers constitutive activation signals to the infected T cell. Therefore, we
378 investigated the effect of Nef on activation pathways downstream of those signaling
379 molecules. To this end, we analyzed the expression of a battery of early and late activation
380 genes in T cells infected with HIV-1 WT or Nef-deficient viruses, or in Nef-expressing cells.

381 Jurkat T cells were infected with HIV-1 WT and Δ Nef viruses and RT-qPCR analysis
382 was performed on non-stimulated cells, in order to estimate the potential effects of Nef on
383 constitutive T cell activation, independently of TCR stimulation. Among the genes
384 investigated, the immediate-early activation genes *FOS* and *JUN* (52) were upregulated upon
385 HIV-1 infection with respect to their basal state in cells infected by WT virus, but to a lesser
386 extent in those infected by Δ Nef virus (Fig. 6A). In contrast, *MYC* basal expression was
387 equally inhibited by both WT and Δ Nef viruses (Fig. 6A). However, the expression of two
388 target genes regulated by the NF κ B signaling pathway, I κ B α (*NFKB1A*) and TNF α induced
389 protein 3 (*TNFAIP3*) (53, 54) was barely changed (Fig. 6B). In addition, we found the
390 expression of several late T cell activation genes, namely *IL2*, *IL2RA* (CD25) and *IFNG*

391 (IFN γ), significantly increased in cells infected by HIV-1 WT, and to a lesser extent in those
392 infected with Δ Nef viruses (Fig. 6C).

393 To further investigate whether Nef expression was sufficient to induce those effects,
394 Jurkat cells were transfected with GFP or Nef-GFP expression vectors and sorted by FACS.
395 GFP and Nef-GFP expressing cells were then assayed for their expression of some of the
396 early and late activation genes referred above (Fig. 6D). The activation trend was confirmed,
397 *JUN* and *FOS* were upregulated by Nef, while *TNFAIP3* and *NFKBIA* gene expression were
398 not significantly changed. Finally, no significant variation of *MYC* expression was observed
399 in Nef expressing cells, in agreement with the Nef-independent inhibitory effect of HIV-1
400 virus infection.

401 Therefore, HIV-1 infection enhances the expression of several early and late activation
402 genes, in a Nef-dependent manner. The effect of Nef was different from gene to gene,
403 suggesting a variable influence of Nef and other viral proteins.

404

405 **Nef-induced accumulation of Lck in intracellular compartments is partly neutralized by** 406 **Rab11-FIP3 depletion and overcomes Nef-induced transcriptional effects**

407 To test whether the activation events induced by HIV-1 Nef were due to the formation
408 of the Nef-induced endosomal Lck compartment, we took advantage of our previous findings
409 showing that Lck is associated with Rab11⁺ endosomes, whose centripetal movement and
410 localization in the pericentrosomal zone are regulated by the Rab11-FIP3 effector protein
411 (from here on called FIP3) (28). Moreover, modification of Rab11 endosomal traffic by the
412 depletion of FIP3 inhibits Lck-mediated T cell signaling events, even in non-stimulated cells
413 (28). Interestingly, FIP3 overexpression induces Lck intracellular accumulation in a similar
414 fashion than Nef (17, 28). In contrast, FIP3 depletion has the opposite effect, dispersing
415 Rab11 endosomes carrying Lck all over the cytoplasm (28). Therefore, we tested whether
416 FIP3 silencing could overcome Lck intracellular accumulation induced by Nef, as well as its
417 potential functional effects on early and late gene expression.

418 As observed previously on the Lck pericentrosomal compartment in non-infected cells
419 (28), FIP3 silencing dispersed the Nef-induced Lck/pZAP70 pericentrosomal accumulation,
420 which became more fragmented and spread over the cytoplasm, as assessed by the
421 distribution of Lck and pZAP70 in the pericentrosomal cytoplasmic area (Fig. 7 A, 7B).

422 We next investigated the effect of FIP3 silencing on HIV-1 Nef-induced upregulation of
423 some of the above-mentioned genes. We used two siRNA oligonucleotides directed to distinct
424 sequences and displaying different silencing efficiencies, siFIP3-2 being more efficient than
425 siFIP3-1 (Fig. 8A top), as we previously reported (28, 31). Note that FIP3 has two isoforms of
426 slightly different electrophoretic mobility (Fig. 8A, double arrow head): siFIP3-1
427 preferentially silenced, though partially, the one of higher molecular mass, whereas siFIP3-2
428 silenced both. In cells transfected with si-control, infection with HIV-1 WT viruses led to
429 upregulation of *JUN*, *FOS*, *IFNG* and *IL2*, genes as described above, that was significantly
430 lower in cells infected with Nef-deficient virus (Fig. 8B, 8C). Interestingly, FIP3 silencing
431 counteracted HIV-1-WT-induced gene upregulation reducing the differences between HIV-1
432 WT and Nef-deficient viruses to lower or non-significant levels in cells silenced with siFIP3-
433 1 and siFIP3-2, respectively (Fig. 8B, 8C, white and grey histogram). Of note is that FIP3
434 silencing did not alter the percentage of infected cells (Fig. 8D) or Nef levels in cell extracts,
435 but slightly reduced the level of the p24 capsid protein (Fig. 8A, 8D).

436 These data indicate that: i) the expression of several of the genes analyzed depends in
437 part on the appropriate regulation of the recycling endosomal compartment controlled by
438 Rab11-FIP3; ii) HIV-1 exacerbates the function of this physiological compartment, in a Nef-
439 dependent manner, increasing the expression of these various genes; iii) perturbation of this
440 compartment by FIP3 silencing counteracts, in a dose-dependent manner, the effects of Nef,
441 reducing gene expression of HIV-1-WT-infected cells to the levels of cells infected with Nef-
442 deficient viruses.

443

444 **Nef sequesters Rac1 in its intracellular compartment and modulates Rac1-mediated T** 445 **cell spreading**

446 In addition to Lck and several of its substrates, we found the GTPase Rac1 concentrated
447 in a pericentrosomal compartment in a Nef-dependent fashion (Fig. 1 B, D). To better define
448 the intracellular compartment in which Nef retains Rac1, we expressed Nef-GFP in Jurkat and
449 primary CD4⁺ T cells and analyzed its relative localization to endogenous Rac1. In control
450 cells expressing GFP, Rac1 is localized at the plasma membrane, in the cytosol, and to a
451 lesser extent in pericentrosomal endosomes, likely corresponding to Rab11⁺ endosomes, as
452 we previously described (31) (Fig. 9A top). In Nef-GFP expressing cells, Rac1 was massively
453 localized in an intracellular compartment that extensively colocalized with Nef (Fig. 9A
454 bottom, 9C). Similar results were found in primary human CD4⁺ T cells transfected with Nef-

455 GFP (Fig. 9B, 9C), although the intracellular compartment was less well spatially resolved
456 due to the smaller cytoplasmic volume of primary T cells.

457 T cell membrane protrusions formed during T cell spreading and immunological
458 synapse formation are reminiscent of lamellipodium structures observed in migrating cells
459 (55), whose formation depends on Rac1 (56). Moreover, we have recently shown that Rac1 is
460 associated with Rab11⁺ endosomes and its subcellular localization is controlled by FIP3.
461 Thus, FIP3-silenced T cells lose the Rac1/Rab11 pericentrosomal compartment, which gets
462 fragmented and spreads all over the cytoplasm. Conversely, FIP3 overexpression induces the
463 accumulation of Rac1 in the Rab11⁺ pericentrosomal compartment (31), somehow
464 reminiscent of Nef effect on Rac1 intracellular localization (Fig. 2C, 9A, 9B). Rab11-
465 mediated Rac1 traffic controls Rac1 functions in T cells. In particular, we showed that T cell
466 capacity to spread on surfaces was exacerbated, both in the presence and absence of TCR
467 stimulation or integrin adhesion (i.e. T cells spreading on poly-lysine). Therefore, we
468 analyzed to what extent FIP3 silencing could compensate Nef-induced Rac1 concentration in
469 the pericentrosomal compartment, and whether Nef was still capable to sequester Rac1 in
470 FIP3-silenced cells. We observed that Rac1 intracellular dispersion in FIP3-silenced / Nef-
471 expressing cells was less efficient than the one we previously observed in control cells not
472 expressing Nef (31), and did not significantly altered Nef and Rac1 colocalization (Fig. 9D-
473 9F).

474 We then investigated whether Nef has an effect on T cells spreading on poly-lysine,
475 which we showed was enhanced in FIP3-silenced cells (31). Therefore, we transfected Jurkat
476 T cells with GFP or Nef-GFP together with si-control or siFIP3 oligonucleotides and analyzed
477 the capacity of cells to spread on poly-lysine. We used poly-lysine as adhesion substrate in
478 order to analyze the effects due to Rac1 and not those potentially involving Lck signaling in T
479 cells spreading on anti-CD3, a process reported to be affected by Nef (10). We observed that
480 Nef expression did not have a significant effect on si-control-treated T cell spreading on poly-
481 lysine, but significantly inhibited the enhancing effect of FIP3 silencing, especially at late
482 times (Fig. 9G, 9H, 15 min).

483 Altogether, these data indicate that the Nef subversion of Rac1 endosomal traffic and
484 Rac1 sequestering in the Nef intracellular compartment modulates Rac1-mediated actin
485 remodeling that supports TCR signaling-independent T cell spreading.

486

487

488 **Discussion**

489 Under physiological conditions, the endosomal traffic of TCR and several of its
490 proximal signaling molecules is crucial for immunological synapse formation and T cell
491 activation. At least three main functions for this molecular traffic have been proposed: first,
492 the targeting of TCR and signaling molecules to the immunological synapse allowing the
493 generation of signaling complexes at the synaptic plasma membrane (2, 20, 21, 23, 25, 26, 30,
494 57); second, the delivery of signaling complexes to endosomes to sustain T cell activation
495 (58); third, the removal of TCRs and signaling molecules from the synaptic plasma membrane
496 in order to down regulate T cell activation (59-61). During HIV-1 infection, the viral protein
497 Nef appears to specifically hijack some of these endosomal pathways, perturbing Lck
498 intracellular traffic with several opposite effects reported: first, to limit Lck clustering and
499 tyrosine phosphorylation of signaling adaptors at the immunological synapse (17, 18); second,
500 to increase the sensitivity of the Ras-Erk and calcium signaling pathways leading to NFAT
501 activation and IL2 production in response to TCR and CD28 stimulation (16, 19, 62-67). The
502 influence of HIV-1 infection and Nef expression on other components of the T cell activation
503 molecular machinery remains, however, poorly defined.

504 Here, we show that HIV-1 infection induces the accumulation of Lck and Rac1 in a
505 pericentrosomal vesicular compartment. Nef is necessary to induce this double accumulation,
506 but the differences between WT and Δ Nef infected cells do not allow us to ensure a full
507 dependence on Nef expression. Other viral proteins might also be involved. Nevertheless, Nef
508 expression alone is enough to induce these effects. Indeed, Nef appears to finely assemble an
509 “autonomous endosomal signaling compartment” that gathers activation-competent forms
510 (i.e. phosphorylated at key Tyr residues) of several TCR-CD3 and CD28 proximal signaling
511 molecules. This compartment includes the phosphorylated active form of Lck, together with
512 pTCR ζ , pZAP70, pSLP76 and pVav1, but not pLAT. Interestingly, Lck, TCR ζ and LAT are
513 associated with spatially adjacent but distinct endosomal compartments (21, 25, 26, 28),
514 while, ZAP70, SLP76 and Vav1 are not associated with endosomes (68) (and our unpublished
515 data). Therefore, the Nef-induced signaling compartment seems not to be just the
516 consequence of the general perturbation of endosomal traffic. Rather, our data are consistent
517 with Nef specifically altering Lck and TCR ζ endosomal traffic, concentrating both proteins in
518 pericentrosomal endosomes, and favoring TCR ζ phosphorylation. In addition, the reported

519 interactions of Nef with Lck (69) and TCR ζ (70) might also contribute to generate this
520 compartment. In turn, locally phosphorylated TCR ζ , would bind ZAP70, favoring its
521 concentration in that compartment, ZAP70 autophosphorylation, and ZAP70 phosphorylation
522 and activation by Lck (4). It is tempting to speculate that Nef could stabilize a transient
523 physiological intermediate signaling compartment (58) providing steady activation signals to
524 the infected cell. To test this hypothesis, we crosslinked CD3 and CD28 and followed the
525 potential generation of an enhanced Lck endosomal compartment containing phosphorylated
526 Lck substrates. We could not detect increased accumulation of Lck or pZAP70 in the
527 pericentrosomal area at activation time points between 5 and 30 min in which pZAP70 and
528 TCR ζ phosphorylation occurs (28), together with TCR-CD3 internalization (20),
529 (Supplemental Fig. 2A, 2B). Rather, the Lck endosomal compartment appeared to lose
530 intensity, as we previously reported (25). This indicates that a translocation of Lck to the
531 plasma membrane occurs, instead of Lck endosomal enrichment.

532 In contrast to what occurs at the immunological synapse plasma membrane, endosome-
533 associated active ZAP70 seems not to be able to phosphorylate endosomal LAT.
534 Nevertheless, pSLP76 concentrates there. Therefore, pSLP76 recruitment to the Nef-induced
535 signaling compartment would not occur *via* pLAT (3). The lack of local formation of optimal
536 amplification complex formed by pLAT and pSLP76 (3) may explain why the constitutive
537 activation of genes induced by Nef is relatively weak (1.5-4 fold higher than the expression of
538 non-infected cells), as compared with that induced by TCR-CD28 stimulation, which
539 generally leads to higher gene expression levels (4-100 fold higher than the expression of
540 non-stimulated cells (28). Instead of pLAT, the interaction of SLP76 with Vav1 (71) could
541 account for SLP76 recruitment, but how these two molecules are recruited remains unknown.
542 It has been reported that Nef interacts with Vav1 in cholesterol and sphingolipids-enriched
543 (detergent insoluble) membrane microdomains (8, 9, 11). These membrane microdomains
544 also continuously cycle between the plasma membrane and the endosomal compartment and
545 could help Vav1 concentration in the pericentrosomal region close to Lck. It is tempting to
546 speculate that while TCR + CD28 induce a strong response leading to proliferation, Nef does
547 not generate a proliferation signal, but rather a mild survival signal that may favor virus
548 replication.

549 The kinetics of Lck and Rac1 accumulation in the pericentrosomal compartment upon
550 HIV-1 infection remain not resolved. The difficulty to detect low levels of Nef expression by
551 immunofluorescence and confocal microscopy, together with intrinsic variability of Lck and

552 Rac1 concentration in the pericentrosomal compartment in non-infected cells make these
553 quantitative measurements at present poorly reliable (our unpublished data).

554 We have identified several early and late activation genes that are differentially
555 regulated during HIV-1 infection in a partly Nef-dependent fashion, even in the absence of
556 TCR stimulation. Thus, *FOS* and *JUN* were upregulated by HIV-1 infection, in a partly Nef-
557 dependent manner. In contrast, *MYC* expression was inhibited, although in a Nef-independent
558 manner. Finally, *NFKBIA* and *TNFAIP3* remained non-significantly changed. This is
559 consistent with previous reports proposing a Nef-mediated modulation of the Ras-Erk,
560 calcium and NFAT signaling pathway with no effect on NF- κ B (19, 62-64, 72). In addition,
561 we observed that several late activation genes, like *IL2*, *IL2RA* and *IFNG* were upregulated in
562 HIV-1 infected cells in a partly Nef-dependent manner. The extent of upregulation and Nef
563 dependence varies among the different genes, suggesting that other HIV-1 proteins may
564 contribute to these effects by this or different mechanisms. Further evidence for Nef
565 dependency of HIV-1-infected cells was the observations that Nef expression by itself
566 increased *JUN* and *FOS* gene expression, without affecting *MYC*, *NFKBIA* and *TNFAIP3*.

567 While our data herein show that HIV-1 infection increases the expression of these
568 various genes independently of TCR stimulation, other authors have shown that Nef
569 expression enhances TCR-CD28 stimulation (16, 19, 62-67). In our case, we cannot rule out
570 that TCR-independent co-stimulation *via* T cell-T cell interaction occurs and contributes to
571 the observed effects. Under physiological conditions, infected cells might get mild
572 stimulations from other cells in lymphoid organs that may cooperate with the Nef-induced
573 compartment to activate infected cells.

574 We have previously shown that Rab11 endosomal traffic is key for Lck and Rac1
575 regulatory functions in T cells. This mechanism modulates TCR signaling and Rac1-mediated
576 actin cytoskeleton remodeling, both important during immunological synapse formation and
577 T cell activation leading to cytokine production (28, 31, 32). Interestingly, Nef mimics FIP3
578 overexpression in its ability to accumulate Lck and Rac1 in the pericentrosomal compartment.
579 The resemblance of effects of Nef and FIP3 overexpression on Lck and Rac1 endosomal
580 traffic is striking and suggest a common mechanism involving Rab11-driven endosomal
581 traffic. For instance, both proteins affect transferrin and transferrin receptor endosomal traffic
582 (34, 73). Moreover, both proteins interact with members of the exocyst complex that regulates
583 vesicle tethering to the plasma membrane and may affect endosomal traffic (74, 75).
584 Conversely, Nef has the opposite effect of FIP3 silencing, enhancing the phosphorylation of

585 some Lck substrates, and counteracting the effect of FIP3 silencing on T cell spreading.
586 Altogether, these data indicate that Nef hijacks the endosomal traffic of Lck and Rac1 to
587 modulate, in an opposite manner, signaling- and actin cytoskeleton-mediated T cell functions.
588 This combined mechanisms may account in part for the reported multiple and sometimes
589 contradictory effects of HIV-1 infection and Nef expression on T cell activation (16), as well
590 as Nef effects on T cell actin cytoskeleton, influencing T cell spreading, cell shape changes
591 and migration (9, 10, 13, 14, 76). Additionally, the Nef effects we describe here may
592 complement other reported mechanisms involving Nef interactions with some signaling and
593 cytoskeleton regulators (16). Finally, Pan et al (19) reported that Nef-induced intracellular
594 retention of Lck could be counteracted by the overexpression of Unc119, a protein also
595 involved in Lck traffic *via* the Rab11 endosomal compartment and in Lck activation (22, 77),
596 further supporting the effect of Rab11 traffic in the effects of Nef on Lck.

597 FIP3 silencing affects gene expression in both non-infected and HIV-1-infected cells
598 and balances the differences between cells infected with HIV-1 WT and Nef-deficient viruses.
599 This is consistent with the idea that HIV-1 hijacks *via* Nef signaling mechanisms existing in
600 non-infected T cells, exacerbating them to produce higher basal levels of some transcription
601 factors (i.e. Fos and Jun) and cytokines (i.e. IFN γ and IL2). This may contribute to an
602 equilibrium between the virus and the infected cell favoring virus replication. In this line,
603 Nef-induced modulation of T cell endosomal and Lck traffic was reported to contribute to
604 virus replication (19, 34). Finally, the subtle relocalization of part of the TCR and CD28
605 signaling machinery might be important for specific HIV-1 effects on apoptosis, or in the
606 process of reprogramming infected cells to quiescence, but this will need further investigation
607 (78).

608 We observed that Nef recruits Rac1 in a compartment that overlaps and colocalizes with
609 Nef more extensively than Lck and the other recruited signaling molecules. This is consistent
610 with an interaction between Nef and Rac1 as shown by others (11, 79). Rac1 and its GEF
611 activator Vav1 have two related functions in T cells, to transduce TCR and CD28 activation
612 signals and to regulate actin cytoskeleton dynamics. In this line, previous reports proposed
613 that Vav1 and Rac1 are involved in Nef-mediated activation of PAK2 (8, 11) and may
614 enhance Ras-Erk and JNK signaling pathways (9, 64). In some of these reports, detergent-
615 insoluble membrane microdomains were suggested to be involved but the two mechanisms
616 would not be exclusive, since membrane microdomains transit through recycling endosomes.
617 Interestingly, we did not observe relocalization of active-phosphorylated forms of Erk or

618 JNK. However, according to the above-cited reports, these kinases are more prone to be
619 activated in Nef-expressing cells when the TCR is engaged. Therefore, we could speculate
620 that the Nef-induced endosomal signaling compartment facilitates the delivery of activation
621 signals to these kinases without concentrating them in this compartment, and leading to
622 increase transcription of cytokine genes, as we show here.

623 We could not elucidate in our study whether Nef can relocalize other Rho-family
624 GTPases, as Rho and Cdc42, because of lack of performing antibodies able to detect
625 endogenous proteins. Worth noting, Rauch et al. reported that Rac1, Cdc42 and Vav1 are
626 recruited to Nef-PAK2 complexes within detergent-insoluble membrane microdomains. They
627 proposed that this recruitment may contribute to Nef effects on T cell activation (11).
628 However, the subcellular localization of the reported complexes appears very different than
629 the Rac1-Nef co-recruitment we describe here. Our data indicate that Rac1 sequestering by
630 Nef is inhibitory for Rac1-mediated cytoskeletal rearrangements leading to T cell spreading.
631 This could also explain the modulatory effect of Nef on T cell shape and migration reported
632 by others (12-14, 76). Therefore, different localizations of Rac1 with respect to Nef might
633 lead to distinct opposite effects. Localization in membrane microdomains might favor
634 signaling, whereas endosomal sequestering might have a dual effect, enhance the Vav1-Rac1
635 signaling pathway and inhibit Rac1-mediated actin cytoskeleton reorganization, as shown
636 here on T cell spreading.

637 In conclusion, this work provides new insights into the understanding of HIV-1 host T
638 cell interactions, *via* the subtle modulation of the endosomal traffic of signaling and
639 cytoskeleton regulators. The two mechanisms are likely different and lead to opposite outputs.
640 Our findings may be the reflect of Nef effects at various steps of the virus life cycle: first,
641 during early phases of infection, in which virus-borne Nef enters the target cell and may cause
642 subcellular local effects on signaling or cytoskeleton; second, during HIV-1 genome
643 transcription in which Nef is expressed from the integrated viral genome, causing more
644 general effects in the infected cells together with other viral proteins; third, Nef could affect
645 bystander cells to which it could be transferred from infected cells, causing Nef specific
646 effects. Finally, although our work largely focused on Nef-dependent effects, our data show
647 that other viral proteins may have significant effects on T cell signaling, using perhaps
648 complementary mechanisms. Finally, Nef induced reorganization of the recycling endosomal
649 compartment an as a consequence the proteins transported by these endosomes, may
650 contribute to the effect of Nef in virus replication as indicated by previous reports (19, 34).

653

654 **Acknowledgments**

655 We thank the Photonic BioImaging UTechS microscopy core facility at the Institut
656 Pasteur for microscopy and technical support, the Cytometry and Biomarkers UTechS core
657 facility at the Institut Pasteur for flow cytometry, cell sorting and technical support, the
658 French Blood Bank (Etablissement Francais du Sang) and the ICAReB (Clinical Investigation
659 and Access to Biological Resources core facility) team for providing blood from healthy
660 donors and primary T cell samples, respectively. The following reagents were obtained
661 through the NIH AIDS Reagent Program, Division of AIDS, NIAID, NIH: monoclonal
662 antibody to HIV-1 p24 (AG3.0) from Dr. Jonathan Allan (80); anti-HIV-1 Nef monoclonal
663 (6.2) from Dr. Kai Krohn and Dr. Vladimir Ovod (81) and HIV-1SF2 p24 antiserum from
664 DAIDS, NIAID, produced by BioMolecular Technologies. We thank Drs S. Benichou and F.
665 Niedergang (Institut Cochin, Paris); H. Moreaux, A. M. Lennon-Dumenil and S. Agüera-
666 Gonzalez (Institut Curie, Paris); and A. Echard, R. Weil and S. Etienne-Manneville (Institut
667 Pasteur, Paris) for antibodies, expression vectors, and methodological help and advice.

668

669 **Disclosures**

670 The authors have no financial conflict of interest

671

672 **References**

- 673 1. Agüera-Gonzalez, S., J. Bouchet, and A. Alcover. 2015. Immunological Synapse. *eLS*.
674 *John Wiley & Sons, Ltd: Chichester* DOI: 10.1002/9780470015902.a0004027.pub2.
- 675 2. Niedergang, F., V. Di Bartolo, and A. Alcover. 2016. Comparative anatomy of
676 phagocytic and immunological synapses. *Front Immunol* 7: 18 doi
677 10.3389/fimmu.2016.00018.
- 678 3. Acuto, O., V. D. Bartolo, and F. Michel. 2008. Tailoring T-cell receptor signals by
679 proximal negative feedback mechanisms. *Nat Rev Immunol* 8: 699-712.
- 680 4. Malissen, B., and P. Bongrand. 2015. Early T cell activation: integrating biochemical,
681 structural, and biophysical cues. *Annu Rev Immunol* 33: 539-561.
- 682 5. Pereira, E. A., and L. L. daSilva. 2016. HIV-1 Nef: Taking Control of Protein
683 Trafficking. *Traffic* 17: 976-996.
- 684 6. Lehmann, M., D. S. Nikolic, and V. Piguet. 2011. How HIV-1 takes advantage of the
685 cytoskeleton during replication and cell-to-cell transmission. *Viruses* 3: 1757-1776.
- 686 7. Verollet, C., V. Le Cabec, and I. Maridonneau-Parini. 2015. HIV-1 Infection of T
687 Lymphocytes and Macrophages Affects Their Migration via Nef. *Front Immunol* 6:
688 514.
- 689 8. Fackler, O. T., X. Lu, J. A. Frost, M. Geyer, B. Jiang, W. Luo, A. Abo, A. S. Alberts,
690 and B. M. Peterlin. 2000. p21-activated kinase 1 plays a critical role in cellular
691 activation by Nef. *Mol Cell Biol* 20: 2619-2627.
- 692 9. Fackler, O. T., W. Luo, M. Geyer, A. S. Alberts, and B. M. Peterlin. 1999. Activation
693 of Vav by Nef induces cytoskeletal rearrangements and downstream effector
694 functions. *Mol Cell* 3: 729-739.
- 695 10. Haller, C., S. Rauch, N. Michel, S. Hannemann, M. J. Lehmann, O. T. Keppler, and O.
696 T. Fackler. 2006. The HIV-1 pathogenicity factor Nef interferes with maturation of
697 stimulatory T-lymphocyte contacts by modulation of N-Wasp activity. *J Biol Chem*
698 281: 19618-19630.
- 699 11. Rauch, S., K. Pulkkinen, K. Saksela, and O. T. Fackler. 2008. Human
700 immunodeficiency virus type 1 Nef recruits the guanine exchange factor Vav1 via an
701 unexpected interface into plasma membrane microdomains for association with p21-
702 activated kinase 2 activity. *J Virol* 82: 2918-2929.
- 703 12. Stolp, B., L. Abraham, J. M. Rudolph, and O. T. Fackler. 2010. Lentiviral Nef
704 proteins utilize PAK2-mediated deregulation of cofilin as a general strategy to
705 interfere with actin remodeling. *J Virol* 84: 3935-3948.
- 706 13. Stolp, B., M. Reichman-Fried, L. Abraham, X. Pan, S. I. Giese, S. Hannemann, P.
707 Goulimari, E. Raz, R. Grosse, and O. T. Fackler. 2009. HIV-1 Nef interferes with host
708 cell motility by deregulation of Cofilin. *Cell Host Microbe* 6: 174-186.
- 709 14. Nobile, C., D. Rudnicka, M. Hasan, N. Aulner, F. Porrot, C. Machu, O. Renaud, M. C.
710 Prevost, C. Hivroz, O. Schwartz, and N. Sol-Foulon. 2010. HIV-1 Nef inhibits ruffles,
711 induces filopodia, and modulates migration of infected lymphocytes. *J Virol* 84: 2282-
712 2293.
- 713 15. Abraham, L., and O. T. Fackler. 2012. HIV-1 Nef: a multifaceted modulator of T cell
714 receptor signaling. *Cell Commun Signal* 10: 39.
- 715 16. Markle, T. J., M. Philip, and M. A. Brockman. 2013. HIV-1 Nef and T-cell activation:
716 a history of contradictions. *Future Virol* 8.
- 717 17. Thoulouze, M. I., N. Sol-Foulon, F. Blanchet, A. Dautry-Varsat, O. Schwartz, and A.
718 Alcover. 2006. Human immunodeficiency virus type-1 infection impairs the formation
719 of the immunological synapse. *Immunity* 24: 547-561.
- 720 18. Abraham, L., P. Bankhead, X. Pan, U. Engel, and O. T. Fackler. 2012. HIV-1 Nef
721 Limits Communication between Linker of Activated T Cells and SLP-76 To Reduce

- 722 Formation of SLP-76-Signaling Microclusters following TCR Stimulation. *J Immunol*
723 189: 1898-1910.
- 724 19. Pan, X., J. M. Rudolph, L. Abraham, A. Habermann, C. Haller, J. Krijnse-Locker, and
725 O. T. Fackler. 2012. HIV-1 Nef compensates for disorganization of the immunological
726 synapse by inducing trans-Golgi network-associated Lck signaling. *Blood* 119: 786-
727 797.
- 728 20. Das, V., B. Nal, A. Dujecourt, M. I. Thoulouze, T. Galli, P. Roux, A. Dautry-
729 Varsat, and A. Alcover. 2004. Activation-induced polarized recycling targets T cell
730 antigen receptors to the immunological synapse; involvement of SNARE complexes.
731 *Immunity* 20: 577-588.
- 732 21. Anton, O., A. Batista, J. Millan, L. Andres-Delgado, R. Puertollano, I. Correas, and
733 M. A. Alonso. 2008. An essential role for the MAL protein in targeting Lck to the
734 plasma membrane of human T lymphocytes. *J Exp Med* 205: 3201-3213.
- 735 22. Gorska, M. M., Q. Liang, Z. Karim, and R. Alam. 2009. Uncoordinated 119 protein
736 controls trafficking of Lck via the Rab11 endosome and is critical for immunological
737 synapse formation. *J Immunol* 183: 1675-1684.
- 738 23. Finetti, F., S. R. Paccani, M. G. Riparbelli, E. Giacomello, G. Perinetti, G. J. Pazour,
739 J. L. Rosenbaum, and C. T. Baldari. 2009. Intraflagellar transport is required for
740 polarized recycling of the TCR/CD3 complex to the immune synapse. *Nat Cell Biol*
741 11: 1332-1339.
- 742 24. Anton, O. M., L. Andres-Delgado, N. Reglero-Real, A. Batista, and M. A. Alonso.
743 2011. MAL Protein Controls Protein Sorting at the Supramolecular Activation Cluster
744 of Human T Lymphocytes. *J Immunol* 186: 6345-6356.
- 745 25. Soares, H., R. Henriques, M. Sachse, L. Ventimiglia, M. A. Alonso, C. Zimmer, M. I.
746 Thoulouze, and A. Alcover. 2013. Regulated vesicle fusion generates signaling
747 nanoterritories that control T cell activation at the immunological synapse. *J Exp Med*
748 210: 2415-2433.
- 749 26. Larghi, P., D. J. Williamson, J. M. Carpier, S. Dogniaux, K. Chemin, A. Bohineust, L.
750 Danglot, K. Gaus, T. Galli, and C. Hivroz. 2013. VAMP7 controls T cell activation by
751 regulating the recruitment and phosphorylation of vesicular Lat at TCR-activation
752 sites. *Nat Immunol* 14: 723-731.
- 753 27. Finetti, F., L. Patrussi, D. Galgano, C. Cassioli, G. Perinetti, G. J. Pazour, and C. T.
754 Baldari. 2015. The small GTPase Rab8 interacts with VAMP-3 to regulate the
755 delivery of recycling T-cell receptors to the immune synapse. *J Cell Sci* 128: 2541-
756 2552.
- 757 28. Bouchet, J., I. Del Rio-Iniguez, E. Vazquez-Chavez, R. Lasserre, S. Aguera-Gonzalez,
758 C. Cucho, M. W. McCaffrey, V. Di Bartolo, and A. Alcover. 2017. Rab11-FIP3
759 Regulation of Lck Endosomal Traffic Controls TCR Signal Transduction. *J Immunol*
760 198: 2967-2978.
- 761 29. Pfisterer, K., F. Forster, W. Paster, V. Supper, A. Ohradanova-Repic, P. Eckerstorfer,
762 A. Zwirzitz, C. Donner, C. Boulegue, H. B. Schiller, G. Ondrovicova, O. Acuto, H.
763 Stockinger, and V. Lekska. 2014. The late endosomal transporter CD222 directs the
764 spatial distribution and activity of Lck. *J Immunol* 193: 2718-2732.
- 765 30. Carpier, J. M., A. E. Zucchetti, L. Bataille, S. Dogniaux, M. Shafaq-Zadah, S. Bardin,
766 M. Lucchino, M. Maurin, L. D. Joannas, J. G. Magalhaes, L. Johannes, T. Galli, B.
767 Goud, and C. Hivroz. 2018. Rab6-dependent retrograde traffic of LAT controls
768 immune synapse formation and T cell activation. *J Exp Med*.
- 769 31. Bouchet, J., I. Del Rio-Iniguez, R. Lasserre, S. Aguera-Gonzalez, C. Cucho, A.
770 Danckaert, M. W. McCaffrey, V. Di Bartolo, and A. Alcover. 2016. Rac1-Rab11-FIP3

- 771 regulatory hub coordinates vesicle traffic with actin remodeling and T-cell activation.
772 *EMBO J* 35: 1160-1174.
- 773 32. Bouchet, J., M. W. McCaffrey, A. Graziani, and A. Alcover. 2016. The functional
774 interplay of Rab11, FIP3 and Rho proteins on the endosomal recycling pathway
775 controls cell shape and symmetry. *Small GTPases*: 1-6.
- 776 33. Greenberg, M. E., A. J. Iafrate, and J. Skowronski. 1998. The SH3 domain-binding
777 surface and an acidic motif in HIV-1 Nef regulate trafficking of class I MHC
778 complexes. *EMBO J* 17: 2777-2789.
- 779 34. Madrid, R., K. Janvier, D. Hitchin, J. Day, S. Coleman, C. Noviello, J. Bouchet, A.
780 Benmerah, J. Guatelli, and S. Benichou. 2005. Nef-induced alteration of the
781 early/recycling endosomal compartment correlates with enhancement of HIV-1
782 infectivity. *J Biol Chem* 280: 5032-5044.
- 783 35. Craig, H. M., M. W. Pandori, and J. C. Guatelli. 1998. Interaction of HIV-1 Nef with
784 the cellular dileucine-based sorting pathway is required for CD4 down-regulation and
785 optimal viral infectivity. *Proc. Natl Acad. Sci. USA* 95: 11229-11234.
- 786 36. Spina, C. A., T. J. Kwok, M. Y. Chowes, J. C. Guatelli, and D. D. Richman. 1994.
787 The importance of nef in the induction of human immunodeficiency virus type 1
788 replication from primary quiescent CD4 lymphocytes. *J Exp Med* 179: 115-123.
- 789 37. Stewart, S. A., D. M. Dykxhoorn, D. Palliser, H. Mizuno, E. Y. Yu, D. S. An, D. M.
790 Sabatini, I. S. Chen, W. C. Hahn, P. A. Sharp, R. A. Weinberg, and C. D. Novina.
791 2003. Lentivirus-delivered stable gene silencing by RNAi in primary cells. *RNA* 9:
792 493-501.
- 793 38. Bouchet, J., I. Del Rio-Iniguez, and A. Alcover. 2017. Imaging Vesicular Traffic at
794 the Immune Synapse. *Methods in molecular biology* 1584: 129-142.
- 795 39. Del Rio-Iniguez, I., J. Bouchet, and A. Alcover. 2017. Studying the Immune Synapse
796 in HIV-1 Infection. *Methods in molecular biology* 1584: 545-557.
- 797 40. Schindelin, J., I. Arganda-Carreras, E. Frise, V. Kaynig, M. Longair, T. Pietzsch, S.
798 Preibisch, C. Rueden, S. Saalfeld, B. Schmid, J. Y. Tinevez, D. J. White, V.
799 Hartenstein, K. Eliceiri, P. Tomancak, and A. Cardona. 2012. Fiji: an open-source
800 platform for biological-image analysis. *Nat Methods* 9: 676-682.
- 801 41. Bolte, S., and F. P. Cordelieres. 2006. A guided tour into subcellular colocalization
802 analysis in light microscopy. *J Microsc* 224: 213-232.
- 803 42. Costes, S. V., D. Daelemans, E. H. Cho, Z. Dobbin, G. Pavlakis, and S. Lockett. 2004.
804 Automatic and quantitative measurement of protein-protein colocalization in live cells.
805 *Biophysical journal* 86: 3993-4003.
- 806 43. Pan, X., M. M. Geist, J. M. Rudolph, W. Nickel, and O. T. Fackler. 2013. HIV-1 Nef
807 disrupts membrane-microdomain-associated anterograde transport for plasma
808 membrane delivery of selected Src family kinases. *Cell Microbiol* 15: 1605-1621.
- 809 44. Kelly, E. E., C. P. Horgan, and M. W. McCaffrey. 2012. Rab11 proteins in health and
810 disease. *Biochem Soc Trans* 40: 1360-1367.
- 811 45. Nika, K., C. Soldani, M. Salek, W. Paster, A. Gray, R. Etzensperger, L. Fugger, P.
812 Polzella, V. Cerundolo, O. Dushek, T. Hofer, A. Viola, and O. Acuto. 2010.
813 Constitutively active Lck kinase in T cells drives antigen receptor signal transduction.
814 *Immunity* 32: 766-777.
- 815 46. Haller, C., S. Rauch, and O. T. Fackler. 2007. HIV-1 Nef employs two distinct
816 mechanisms to modulate Lck subcellular localization and TCR induced actin
817 remodeling. *PLoS ONE* 2: e1212.
- 818 47. Michel, F., G. Mangino, G. Attal-Bonnefoy, L. Tuosto, A. Alcover, A. Roumier, D.
819 Olive, and O. Acuto. 2000. CD28 utilizes Vav-1 to enhance TCR-proximal signaling
820 and NF-AT activation. *J Immunol* 165: 3820-3829.

- 821 48. Boomer, J. S., and J. M. Green. 2010. An enigmatic tail of CD28 signaling. *Cold*
822 *Spring Harb Perspect Biol* 2: a002436.
- 823 49. Swigut, T., N. Shohdy, and J. Skowronski. 2001. Mechanism for down-regulation of
824 CD28 by Nef. *EMBO J* 20: 1593-1604.
- 825 50. Pawlak, E. N., B. S. Dirk, R. A. Jacob, A. L. Johnson, and J. D. Dikeakos. 2018. The
826 HIV-1 accessory proteins Nef and Vpu downregulate total and cell surface CD28 in
827 CD4(+) T cells. *Retrovirology* 15: 6.
- 828 51. Hornstein, I., A. Alcover, and S. Katzav. 2004. Vav proteins, masters of the world of
829 cytoskeleton organization. *Cell Signal* 16: 1-11.
- 830 52. Chauhan, D., S. M. Kharbanda, E. Rubin, B. A. Barut, A. Mohrbacher, D. W. Kufe,
831 and K. C. Anderson. 1993. Regulation of c-jun gene expression in human T
832 lymphocytes. *Blood* 81: 1540-1548.
- 833 53. Rao, N. A., M. T. McCalman, P. Moulos, K. J. Francoijs, A. Chatziioannou, F. N.
834 Kolisis, M. N. Alexis, D. J. Mitsiou, and H. G. Stunnenberg. 2011. Coactivation of
835 GR and NFkB alters the repertoire of their binding sites and target genes. *Genome*
836 *research* 21: 1404-1416.
- 837 54. Altonsy, M. O., S. K. Sasse, T. L. Phang, and A. N. Gerber. 2014. Context-dependent
838 cooperation between nuclear factor kappaB (NF-kappaB) and the glucocorticoid
839 receptor at a TNFAIP3 intronic enhancer: a mechanism to maintain negative feedback
840 control of inflammation. *J Biol Chem* 289: 8231-8239.
- 841 55. Dustin, M. L. 2007. Cell adhesion molecules and actin cytoskeleton at immune
842 synapses and kinapses. *Curr Opin Cell Biol* 19: 529-533.
- 843 56. Rougerie, P., and J. Delon. 2012. Rho GTPases: masters of T lymphocyte migration
844 and activation. *Immunology letters* 142: 1-13.
- 845 57. Purbhoo, M. A., H. Liu, S. Oddos, D. M. Owen, M. A. Neil, S. V. Pagoon, P. M.
846 French, C. E. Rudd, and D. M. Davis. 2010. Dynamics of subsynaptic vesicles and
847 surface microclusters at the immunological synapse. *Sci Signal* 3: ra36.
- 848 58. Yudushkin, I. A., and R. D. Vale. 2010. Imaging T-cell receptor activation reveals
849 accumulation of tyrosine-phosphorylated CD3zeta in the endosomal compartment.
850 *Proc Natl Acad Sci U S A* 107: 22128-22133.
- 851 59. Alcover, A., B. Alarcon, and V. Di Bartolo. 2017. Cell Biology of T Cell Receptor
852 Expression and Regulation. *Annu Rev Immunol*.
- 853 60. Balagopalan, L., V. A. Barr, C. L. Sommers, M. Barda-Saad, A. Goyal, M. S.
854 Isakowitz, and L. E. Samelson. 2007. c-Cbl-mediated regulation of LAT-nucleated
855 signaling complexes. *Mol Cell Biol* 27: 8622-8636.
- 856 61. Barr, V. A., L. Balagopalan, M. Barda-Saad, R. Polishchuk, H. Boukari, S. C.
857 Bunnell, K. M. Bernot, Y. Toda, R. Nossal, and L. E. Samelson. 2006. T-cell antigen
858 receptor-induced signaling complexes: internalization via a cholesterol-dependent
859 endocytic pathway. *Traffic* 7: 1143-1162.
- 860 62. Manninen, A., G. H. Renkema, and K. Saksela. 2000. Synergistic activation of NFAT
861 by HIV-1 nef and the Ras/MAPK pathway. *J Biol Chem* 275: 16513-16517.
- 862 63. Manninen, A., and K. Saksela. 2002. HIV-1 Nef interacts with inositol trisphosphate
863 receptor to activate calcium signaling in T cells. *J Exp Med* 195: 1023-1032.
- 864 64. Schragar, J. A., V. Der Minassian, and J. W. Marsh. 2002. HIV Nef increases T cell
865 ERK MAP kinase activity. *J Biol Chem* 277: 6137-6142.
- 866 65. Witte, V., B. Laffert, O. Rosorius, P. Lischka, K. Blume, G. Galler, A. Stilper, D.
867 Willbold, P. D'Aloja, M. Sixt, J. Kolanus, M. Ott, W. Kolanus, G. Schuler, and A. S.
868 Baur. 2004. HIV-1 Nef mimics an integrin receptor signal that recruits the polycomb
869 group protein Eed to the plasma membrane. *Mol Cell* 13: 179-190.

- 870 66. Schragar, J. A., and J. W. Marsh. 1999. HIV-1 Nef increases T cell activation in a
871 stimulus-dependent manner. *Proc Natl Acad Sci U S A* 96: 8167-8172.
- 872 67. Wang, J. K., E. Kiyokawa, E. Verdin, and D. Trono. 2000. The Nef protein of HIV-1
873 associates with rafts and primes T cells for activation. *Proc Natl Acad Sci U S A* 97:
874 394-399.
- 875 68. Groysman, M., I. Hornstein, A. Alcover, and S. Katzav. 2002. Vav-1 and Ly-GDI,
876 two regulators of Rho GTPases, function cooperatively as signal transducers in T cell
877 antigen receptor-induced pathways. *J. Biol. Chem.* 277: 50121-50130.
- 878 69. Collette, Y., H. Dutartre, A. Benziane, M. Ramos, R. Benarous, M. Harris, and D.
879 Olive. 1996. Physical and functional interaction of Nef with Lck.HIV-1 Nef-induced
880 T cell signaling defects. *J. Biol. Chem.* 271: 6333-6341.
- 881 70. Xu, X. N., B. Laffert, G. R. Screaton, M. Kraft, D. Wolf, W. Kolanus, J.
882 Mongkolsapay, A. J. McMichael, and A. S. Baur. 1999. Induction of Fas ligand
883 expression by HIV involves the interaction of Nef with the T cell receptor zeta chain.
884 *J Exp Med* 189: 1489-1496.
- 885 71. Ksionda, O., A. Saveliev, R. Kochl, J. Rapley, M. Faroudi, J. E. Smith-Garvin, C.
886 Wulfing, K. Rittinger, T. Carter, and V. L. Tybulewicz. 2012. Mechanism and
887 function of Vav1 localisation in TCR signalling. *J Cell Sci* 125: 5302-5314.
- 888 72. Witte, V., B. Laffert, P. Gintschel, E. Krautkramer, K. Blume, O. T. Fackler, and A. S.
889 Baur. 2008. Induction of HIV transcription by Nef involves Lck activation and protein
890 kinase C theta raft recruitment leading to activation of ERK1/2 but not NF kappa B. *J*
891 *Immunol* 181: 8425-8432.
- 892 73. Horgan, C. P., A. Oleksy, A. V. Zhdanov, P. Y. Lall, I. J. White, A. R. Khan, C. E.
893 Futter, J. G. McCaffrey, and M. W. McCaffrey. 2007. Rab11-FIP3 is critical for the
894 structural integrity of the endosomal recycling compartment. *Traffic* 8: 414-430.
- 895 74. Fielding, A. B., E. Schonteich, J. Matheson, G. Wilson, X. Yu, G. R. Hickson, S.
896 Srivastava, S. A. Baldwin, R. Prekeris, and G. W. Gould. 2005. Rab11-FIP3 and FIP4
897 interact with Arf6 and the exocyst to control membrane traffic in cytokinesis. *EMBO J*
898 24: 3389-3399.
- 899 75. Mukerji, J., K. C. Olivieri, V. Misra, K. A. Agopian, and D. Gabuzda. 2012.
900 Proteomic analysis of HIV-1 Nef cellular binding partners reveals a role for exocyst
901 complex proteins in mediating enhancement of intercellular nanotube formation.
902 *Retrovirology* 9: 33.
- 903 76. Stolp, B., A. Imle, F. M. Coelho, M. Hons, R. Gorina, R. Lyck, J. V. Stein, and O. T.
904 Fackler. 2012. HIV-1 Nef interferes with T-lymphocyte circulation through confined
905 environments in vivo. *Proc Natl Acad Sci U S A* 109: 18541-18546.
- 906 77. Gorska, M. M., S. J. Stafford, O. Cen, S. Sur, and R. Alam. 2004. Unc119, a novel
907 activator of Lck/Fyn, is essential for T cell activation. *J Exp Med* 199: 369-379.
- 908 78. Timilsina, U., and R. Gaur. 2016. Modulation of apoptosis and viral latency - an axis
909 to be well understood for successful cure of human immunodeficiency virus. *J Gen*
910 *Virol* 97: 813-824.
- 911 79. Janardhan, A., T. Swigut, B. Hill, M. P. Myers, and J. Skowronski. 2004. HIV-1 Nef
912 binds the DOCK2-ELMO1 complex to activate rac and inhibit lymphocyte
913 chemotaxis. *PLoS Biol* 2: E6.
- 914 80. Simm, M., M. Shahabuddin, W. Chao, J. S. Allan, and D. J. Volsky. 1995. Aberrant
915 Gag protein composition of a human immunodeficiency virus type 1 vif mutant
916 produced in primary lymphocytes. *J Virol* 69: 4582-4586.
- 917 81. Ovod, V., A. Lagerstedt, A. Ranki, F. O. Gombert, R. Spohn, M. Tahtinen, G. Jung,
918 and K. J. Krohn. 1992. Immunological variation and immunohistochemical
919 localization of HIV-1 Nef demonstrated with monoclonal antibodies. *AIDS* 6: 25-34.

921

922 **Footnotes**

923 ¹ Current address: Institut Cochin, INSERM U1016, CNRS UMR8104, Université Paris
924 Descartes, Sorbonne Paris Cité, Paris, France.

925 ² JB and AA contributed equally to this work as senior authors

926

927 ³ This work was supported by grants from the Agence Nationale de Recherche sur le SIDA et
928 les Hépatites Virales (ANRS, Grant AO 2013-02 CSS1 No 1339/14673), Sidaction (Grant
929 VIH20160721001), the Institut Pasteur, INSERM, and the People Programme (Marie
930 Skłodowska-Curie Actions) of the European Union's Seventh Framework Programme (Grant
931 FP7/2007-2013, under the Research Executive Agency Grant agreement No 317057 HOMIN-
932 ITN). The Photonic BioImaging UTechS microscopy facility at the Institut Pasteur is part of
933 the France BioImaging infrastructure supported by Grant ANR-10-INSB-04-01, "Investments
934 for the Future." Personnel's funding was as follows: IdR-I obtained predoctoral funding from
935 the European Union Marie Curie Actions HOMIN-ITN (cited above), Fondation pour la
936 Recherche Médicale and ANRS . IdR-I is a scholar in the Pasteur-Paris University
937 International Doctoral program (PPU); EV-C received postdoctoral funding from Sidaction;
938 JB received postdoctoral funding from ANRS, Roux-Institut Pasteur and Sidaction.

939

940 ⁴ IdRI and EVC design and performed experiments, analyzed data and contributed to
941 manuscript writing. CC provided technical assistance. VdB provided expertise and critically
942 read the manuscript. JB designed and performed experiments, analyzed data and critically
943 read the manuscript. AA conceived the project, designed experiments, analyzed data and
944 wrote the manuscript.

945 ⁵ Abbreviations used in this article: ANRS, Agence Nationale de Recherche sur le SIDA et les
946 Hépatites Virales; ERC, endosomal recycling compartment; FIP3, Rab11 family interacting
947 protein-3; ICAReB, Institut Pasteur Clinical Investigation and Access to Biological
948 Resources; IFT, intraflagellar transport protein; RT-qPCR, retrotranscription quantitative
949 PCR; siRNA, small interfering RNA; WT, wild type.

950

951

952 **Figure. Legends**

953 **Fig. 1: HIV-1-infected cells accumulate Lck and Rac1 in intracellular compartments in a**
954 **Nef-dependent manner**

955 Intracellular localization of endogenous Lck and Rac1 in primary human T cells (**A, B**) or
956 Jurkat T cells (**C, D**). Cells were left uninfected (top panel), or infected with wild type HIV-1-
957 WT (mid panel) or Δ Nef (bottom panels) viruses. Three days post-infection, the subcellular
958 localization of endogenous Lck and Rac1 was analyzed by immunofluorescence and confocal
959 microscopy. Infected cells were identified by the expression of the HIV-1 capsid polypeptide
960 of 24 kDa (p24). Bar, 3 μ m in A, B and 5 μ m in C, D.

961 A z-stack of 0.2 μ m confocal optical sections was acquired for each cell. Three-dimensional
962 (3D) confocal images were post-treated by deconvolution. A 0.4 μ m-thick medial stack is
963 shown. The pericentrosomal vesicular compartment is zoomed at the bottom right-hand
964 corner in the middle column panels. Right column panels show density gradient fluorescent
965 intensities in a color-code display of Lck or Rac1 localization. Images are representative of
966 three experiments.

967

968 **Figure. 2: HIV-1 Nef is sufficient to induce the accumulation of active Lck and Rac1 in**
969 **the endosomal compartment**

970 **A:** Intracellular localization of endogenous Lck and Nef in Jurkat T cells transfected with
971 expression vectors encoding GFP (top) or Nef-GFP (bottom panel). Colocalization between
972 endogenous Lck and GFP or Nef-GFP in the pericentrosomal compartment was assessed by
973 the Pearson's's Correlation Coefficient (R) as described in Materials and Methods.

974 **B:** Intracellular localization of endogenous Lck phosphorylated on the activatory residue
975 Tyr394 (pLck) and total Lck in Jurkat T cells expressing Nef-GFP. Colocalization between
976 pLck and Lck in the pericentrosomal compartment was assessed as in A.

977 **C:** Intracellular localization of endogenous Rac1 and Nef in Jurkat T cells expressing GFP
978 (top) or Nef-GFP (bottom panel). Colocalization between endogenous Rac1 and GFP or Nef-
979 GFP in the pericentrosomal compartment was assessed as in A.

980 **D, E:** Intracellular localization of endogenous Lck and Rab11 (**D**), or Lck and the trans-Golgi
981 network protein TGN46 (**E**) in Jurkat T cells expressing Nef-GFP. Colocalization between
982 endogenous Lck and Rab11 or Lck and TGN46 in the pericentrosomal compartment was
983 assessed as in A.

984 **A-E:** A z-stack of 0.2 μm confocal optical sections was acquired for each cell. 3D confocal
985 images were post-treated by deconvolution. A 0.4- μm -thick medial stack is shown. Bottom
986 right corner of each image corresponds to a zoomed image of the pericentrosomal vesicular
987 compartment of each cell. Bar, 5 μm . Images are representative of three experiments.

988

989 **Figure. 3: The Nef-induced Lck endosomal compartment gathers signaling competent**
990 **phosphorylated forms of TCR ζ , ZAP70, SLP76 and Vav1, but not LAT**

991 **A-E:** Jurkat T cells expressing GFP (top) or Nef-GFP (bottom), in which the localization of
992 endogenous phosphorylated signaling proteins was assessed by immunofluorescence, using
993 antibodies directed to specific phosphotyrosine (pTyr) residues. A z-stack of 0.2 μm -confocal
994 optical sections was acquired for each cell. 3D confocal images were post-treated by
995 deconvolution. A 0.4- μm -thick medial stack is shown. Bottom right corner of each image
996 corresponds to a zoomed image of the pericentrosomal vesicular compartment of each cell.
997 Analysis of colocalization between endogenous Lck and pTyr142-TCR ζ (**A**), pTyr319-
998 ZAP70 (**B**), pTyr191-LAT (**C**), pTyr128-SLP76 (**D**) and pTyr174-Vav1 (**E**) in the
999 pericentrosomal compartment was assessed by the Pearson's Correlation Coefficient (R).
1000 Bar, 5 μm . Images are representative of three experiments.

1001 Right column plots show cell population analyses of R values of the different phospho-
1002 proteins. Each dot corresponds to a different cell. Horizontal bars represent the mean \pm SEM,
1003 Mann-Whitney *U*-test was used. ****, $p < 0.0001$; ***, $p < 0.001$; **, $p < 0.01$; *, $p < 0.05$; non-
1004 significant (ns), $p \geq 0.05$.

1005

1006 **Figure. 4: Recruitment of phosphorylated Zap70 is dependent on Nef's ability to**
1007 **generate the Lck endosomal compartment**

1008 **A:** Intracellular localization of endogenous Lck and phospho-proteins in Jurkat T cells
1009 expressing GFP or Nef-GFP. A z-stack of 1 μm confocal optical sections was acquired for
1010 each cell. Localization of endogenous proteins was assessed by immunofluorescence as in
1011 3A-E. Plots represent the % fluorescence intensity of phospho-proteins in the area
1012 corresponding to the Lck compartment divided by the fluorescence intensity of phospho-
1013 protein in the whole cell area, as described in Methods. Each dot represents one cell.
1014 Horizontal bars represent the mean \pm SEM. Mann-Whitney *U*-test was used. ****, $p < 0.0001$;
1015 ***, $p < 0.001$; **, $p < 0.01$; *, $p < 0.05$; non-significant (ns), $p \geq 0.05$.

1016 **B:** Jurkat T cells expressing Nef PXXP/AXXA-GFP (top) or GFP (bottom), in which the
1017 localization of endogenous Lck and pTyr319-ZAP70 proteins was assessed by
1018 immunofluorescence and confocal microscopy. A z-stack of 0.2 μm -confocal optical sections
1019 was acquired for each cell. 3D confocal images were post-treated by deconvolution. A 0.4-
1020 μm -thick medial stack is shown. Bottom right corner of each image corresponds to a zoomed
1021 image of the pericentrosomal vesicular compartment of each cell. Bar, 5 μm . Images are
1022 representative of three experiments.

1023 **C:** Cell population analysis of colocalization between Lck and pZAP70 in GFP and Nef
1024 PXXP/AXXA-GFP cells in the pericentrosomal compartment was assessed as in 3A-E. Each
1025 dot represents one cell. Horizontal bars represent the mean \pm SEM. Mann-Whitney *U*-test was
1026 used. Non-significant (ns), $p \geq 0.05$.

1027 **D:** Fluorescence intensity levels of pZAP70 in unstimulated Jurkat cells expressing GFP, Nef-
1028 GFP and Nef PXXP/AXXA-GFP cells were analyzed by flow cytometry. Horizontal bars
1029 represent the mean \pm SEM. Data are the mean of three independent biological experiments,
1030 with 2 replicates per experiment. T student test was used. ****, $p < 0.0001$; **, $p < 0.01$; *,
1031 $p < 0.05$.

1032

1033 **Figure. 5: Nef induces the accumulation of CD28 in a pericentrosomal compartment**
1034 **where it partially co-localizes with Rac1, but not with phosphorylated Vav1**

1035 **A:** Intracellular localization of endogenous CD28 in Jurkat T cells expressing GFP (top
1036 panels) or Nef-GFP (bottom panels) were analyzed by immunofluorescence and confocal
1037 microscopy. A z-stack of 0.2- μm -confocal optical sections was acquired for each cell. 3D
1038 confocal images were post-treated by deconvolution. A 0.4- μm -thick medial stack is shown.
1039 Bottom right corner of each image corresponds to a zoomed image of the pericentrosomal
1040 vesicular compartment of each cell. Bar, 5 μm . Images representative of three experiments.

1041 **B:** Cell population analysis of colocalization between Nef-GFP and CD28 in the
1042 pericentrosomal compartment was assessed as in Fig. 3. Each dot represents one cell.
1043 Horizontal bars represent the mean \pm SEM.

1044 **C-F:** Intracellular localization of endogenous pTyr174-Vav1 and CD28 (**C-D**) and Rac1 and
1045 CD28 (**E-F**) in Nef-GFP cells was analyzed by immunofluorescence and confocal
1046 microscopy. A z-stack of 0.2- μm -confocal optical sections was acquired for each cell. 3D
1047 confocal images were post-treated by deconvolution. A 0.4- μm -thick medial stack is shown.

1048 Bottom right corner of each image corresponds to a zoomed image of the pericentrosomal
1049 vesicular compartment of each cell. Bar, 5 μ m. Images representative of three experiments.
1050 Cell population analysis of colocalization between pTyr-174Vav1 and CD28 (**D**) and Rac1
1051 and CD28 (**F**) in the pericentrosomal compartment was assessed as in Fig. 3. Each dot
1052 represents one cell. Horizontal bars represent the mean \pm SEM.

1053

1054 **Figure. 6: Effect of HIV-1 Nef on gene expression**

1055 **A-C:** Jurkat T cells were left uninfected (Ctrl) or infected with HIV-1 WT or Δ Nef viruses.
1056 Two days post-infection, non-stimulated cells were lysed and mRNA expression levels of the
1057 early activation genes *JUN*, *FOS* and *MYC* (**A**), of the NF κ B target genes, *TNFAPI3*, and
1058 *NFKBIA* (**B**), and of the late activation genes, *IL2*, *IFNG* (IFN γ) and *IL2RA* (*CD25*) (**C**) were
1059 assessed by RT-qPCR and normalized to the *B2M* housekeeping gene. Data are the mean \pm
1060 SEM values (n=4) of a representative experiment out of three independent experiments
1061 performed. T student test was used ****, p < 0.0001; ***, p < 0.001; **, p < 0.01; *, p <
1062 0.05; non-significant (ns), p \geq 0.05

1063 **D:** Jurkat T cells were transfected with GFP or Nef-GFP expression vectors. 24h later, GFP
1064 positive cells were sorted, lysed and the mRNA expression levels of *JUN*, *FOS*, *MYC*,
1065 *TNFAPI3* and *NFKBIA* were assessed by RT-qPCR and normalized to the *B2M* housekeeping
1066 gene. Data are the mean of seven independent biological experiments, with four replicates per
1067 experiment. Plots represent mean \pm SEM values (n=28). Mann-Whitney *U*-test was used. ***,
1068 p < 0.001; *, p < 0.05; non-significant (ns), p \geq 0.05.

1069

1070

1071 **Figure. 7: FIP3 silencing disaggregates the Nef-induced Lck compartment**

1072 **A-C:** Jurkat T cells were co-transfected with control (siCtrl) or FIP3 (siFIP3) siRNA
1073 oligonucleotides and with GFP or Nef-GFP expression vectors as described in Methods. Nef-
1074 GFP, endogenous Lck and pTyr319-ZAP70 subcellular localization was analyzed by
1075 immunofluorescence and confocal microscopy. A z-stack of 0.2 μ m confocal optical sections
1076 was acquired for each cell. 3D confocal images were post-treated by deconvolution.

1077 **A:** a 0.4- μ m-thick medial stack is shown. Bar 5 μ m. Images representative of three
1078 experiments.

1079 **B:** Densitometry profiles of pTyr319-ZAP70 across the largest cytoplasmic area, including
1080 plasma membrane and the pericentrosomal Lck compartment, were obtained as described in
1081 Methods. Four representative cells are shown out of twenty analyzed.

1082 **C:** Western Blot analysis of lysates from Jurkat T cells transfected as described in A-C. Blot
1083 shows the band corresponding to FIP3 and β -Tubulin proteins.

1084

1085 **Figure. 8: FIP3 silencing counteracts HIV-1 effects on T cell gene expression**

1086 **A-D:** Jurkat T cells were transfected with siCtrl or siFIP3 oligonucleotides. 36 h later, cells
1087 were left uninfected (Ctrl) or infected with HIV-1 WT or Δ Nef viruses for 36 h, as described
1088 in Materials and Methods.

1089 **A:** Western Blot analysis of lysates from control and infected Jurkat T cells. Bands
1090 corresponding to FIP3, and Nef and p24 viral proteins and GAPDH as internal control are
1091 depicted. Note that FIP3 has two isoforms of slightly different electrophoretic mobility
1092 (double arrow head). SiFIP3-1 preferentially silenced, though partially, the one of higher
1093 molecular mass, whereas siFIP3-2 silenced both more efficiently.

1094 **B-C:** Infected cells were lysed and mRNA levels of *JUN*, *FOS* (**B**), *NFKBIA*, *IFNG* and *IL2*
1095 (**C**) were assessed by RT-qPCR and normalized to the *B2M* housekeeping gene mRNA. Data
1096 show the mean \pm SEM values with n=4 from a representative experiment out of three
1097 independent experiments. Two-Way ANOVA was used. For clarity only statistics between
1098 the WT and Δ Nef conditions are shown. ****, $p < 0.0001$; **, $p < 0.01$; non-significant (ns),
1099 $p \geq 0.05$

1100 **D:** KC57-FITC labelled antibody was used to analyze infection levels (HIV-1 proteins 55, 39,
1101 33 & 24 kDa of core antigen) by flow cytometry.

1102

1103

1104 **Figure. 9: Nef expression sequesters Rac1 and inhibits Rac-1-dependent T cell spreading**
1105 **induced by FIP3 silencing**

1106 **A, B:** Jurkat T cells (**A**) or CD4 primary T cells (**B**) were transfected with GFP (top) or Nef-
1107 GFP (bottom) expression vectors and the intracellular localization of endogenous Rac1 was
1108 analyzed by immunofluorescence and confocal microscopy. A z-stack of 0.2- μ m-confocal
1109 optical sections was acquired for each cell. 3D confocal images were post-treated by
1110 deconvolution. A 0.4- μ m-thick medial stack is shown. Bottom right corner of each image

1111 corresponds to a zoomed image of the pericentrosomal vesicular compartment of each cell.
1112 Bar 5 μm (A) and 3 μm (B). Images representative of three experiments.
1113 **C:** Cell population analysis of colocalization between endogenous Rac1 and Nef-GFP in the
1114 Nef-induced compartment assessed by the Pearson's Correlation Coefficient (R). Each dot
1115 represents one cell. Horizontal bars represent the mean \pm SEM.
1116 **D-F:** Jurkat T cells were co-transfected with control (siCtrl) or FIP3 (siFIP3) siRNA
1117 oligonucleotides and GFP or Nef-GFP expression vectors, as described in Methods.
1118 Subcellular localization of Nef-GFP, and endogenous Rac1 was analyzed by
1119 immunofluorescence and confocal microscopy. A z-stack of 0.2 μm confocal optical sections
1120 was acquired for each cell. 3D confocal images were post-treated by deconvolution.
1121 **D:** A 0.4- μm -thick medial stack is shown. Bottom right corner of each image corresponds to a
1122 zoomed image of the pericentrosomal vesicular compartment of each cell. Representative of
1123 three experiments. Bar 5 μm .
1124 **E:** Densitometry profiles across cells including plasma membrane and the pericentrosomal
1125 Nef and Rac1 compartment were obtained as described in Methods. Four representative cells
1126 are shown out of twenty analyzed.
1127 **F:** Cell population analysis of colocalization between Nef-GFP and Rac1 in the Nef-induced
1128 compartment was assessed as in C. Each dot represents one cell. Horizontal bars represent the
1129 mean \pm SEM. Mann-Whitney *U*-test was used. Non-significant (ns), $p \geq 0.05$.
1130 **G:** Jurkat T cells were co-transfected with control (siCtrl) or FIP3 (siFIP3) siRNA
1131 oligonucleotides and GFP or Nef-GFP expression vectors, as described in Methods. Cells
1132 were allowed to spread on poly-lysine-coated coverslips for 2, 5 or 15 min, and F-actin was
1133 stained using a fluorescent-labelled Phalloidin. Cells were analyzed by confocal microscopy.
1134 Cell contact surface was measured using ImageJ, as described in Methods. A z-stack of 0.2
1135 μm confocal optical sections was acquired for each cell. 3D confocal images were post-
1136 treated by deconvolution. A 0.4- μm thick stack at the contact surface is shown. Bar 3 μm .
1137 Images representative of three experiments
1138 **H:** Cell population analysis dot plots displaying spreading area values at 5 and 15 min. Each
1139 dot represents one cell. Horizontal bars represent the mean \pm SEM. Mann-Whitney *U*-test was
1140 used. ****, $p < 0.0001$; non-significant (ns), $p \geq 0.05$.
1141

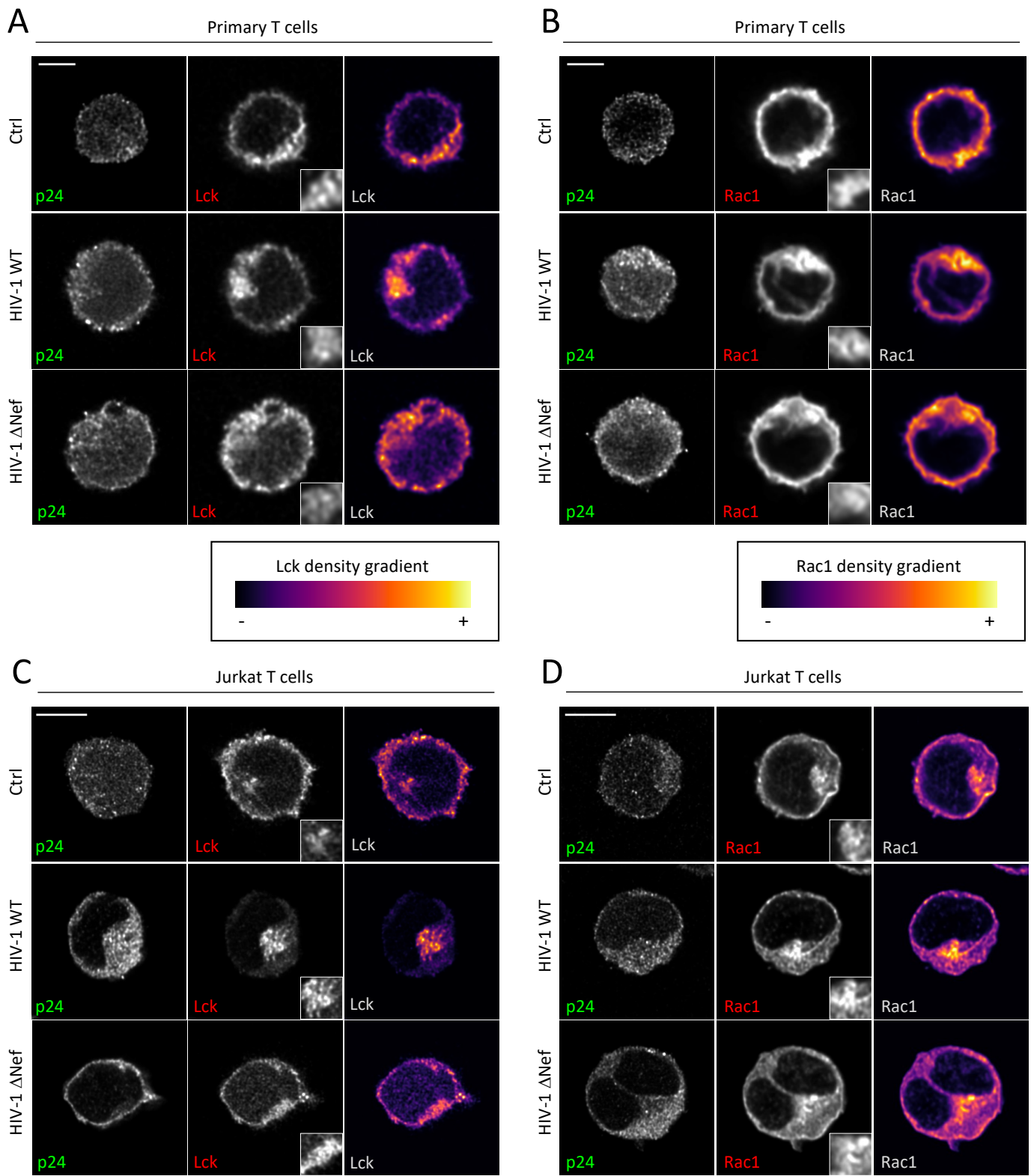


Figure 1

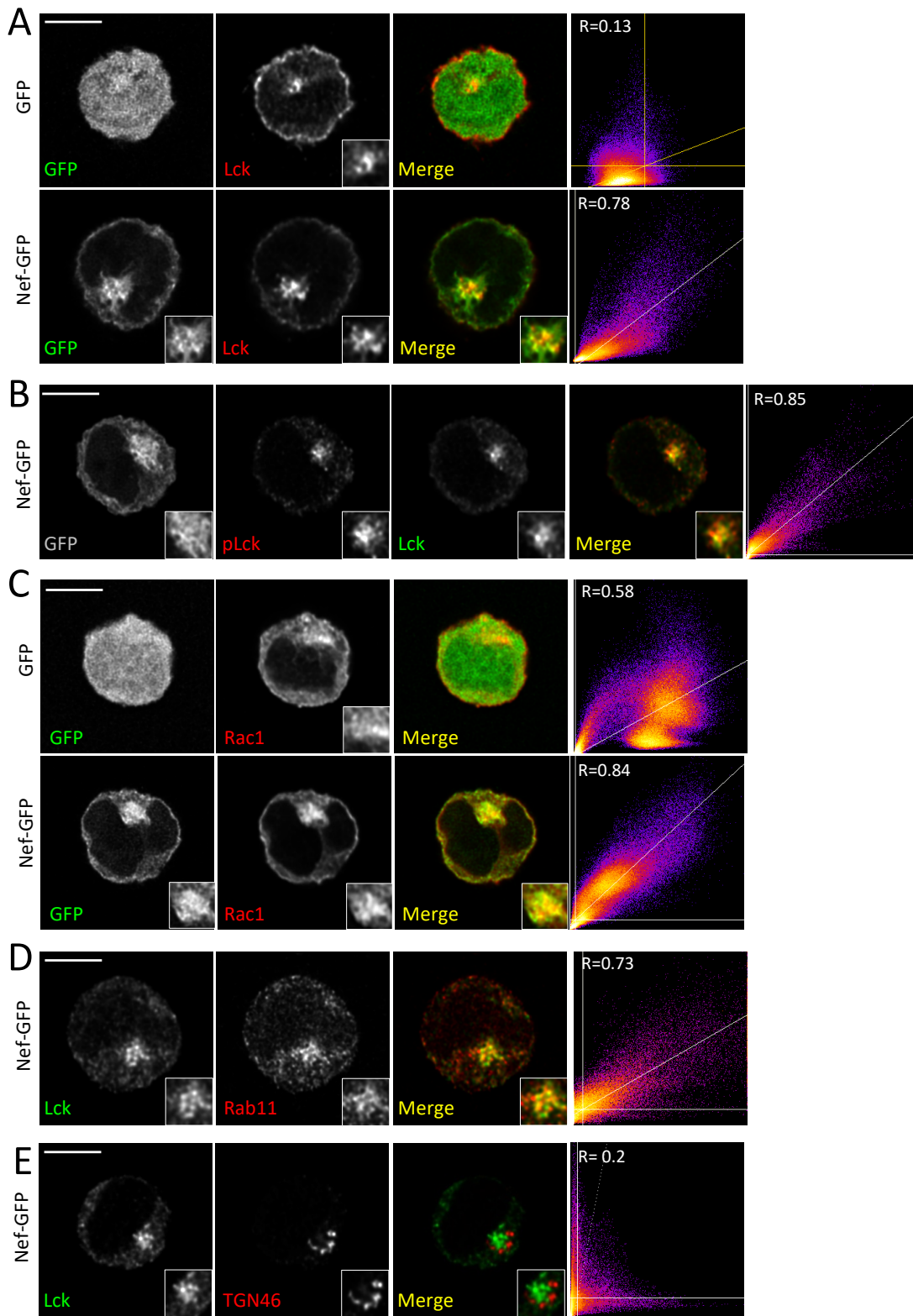


Figure 2

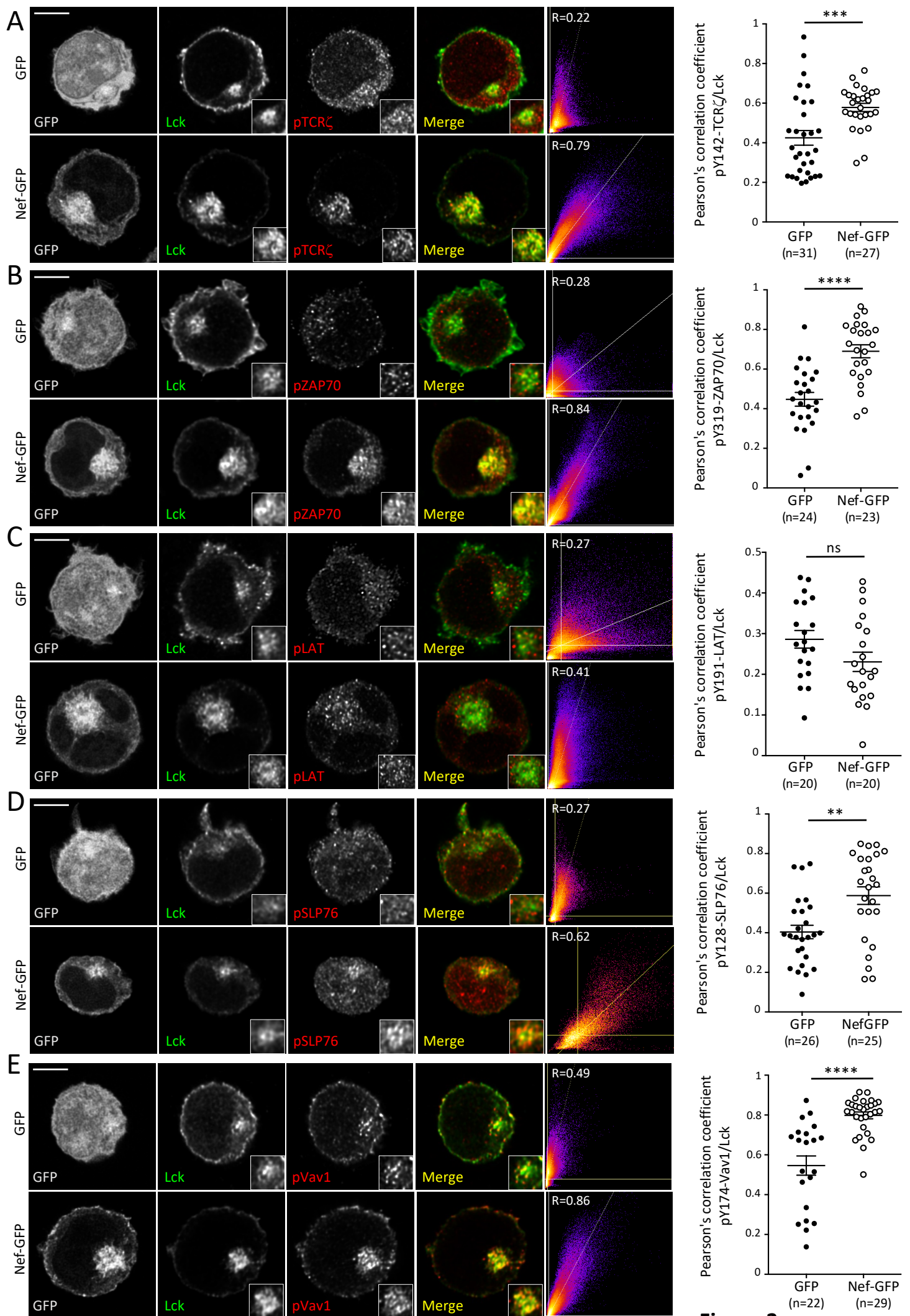


Figure 3

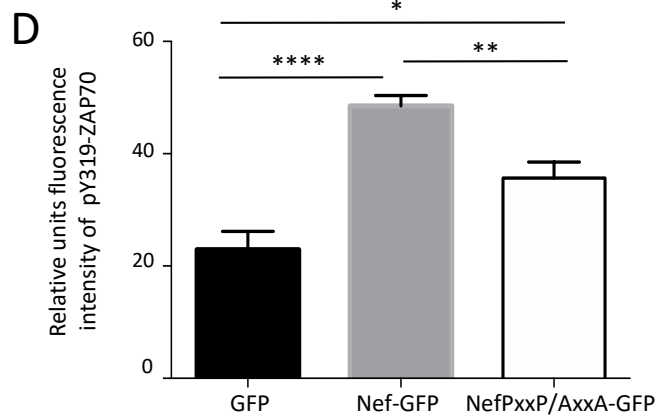
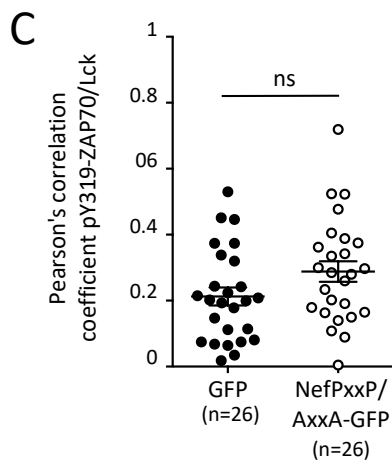
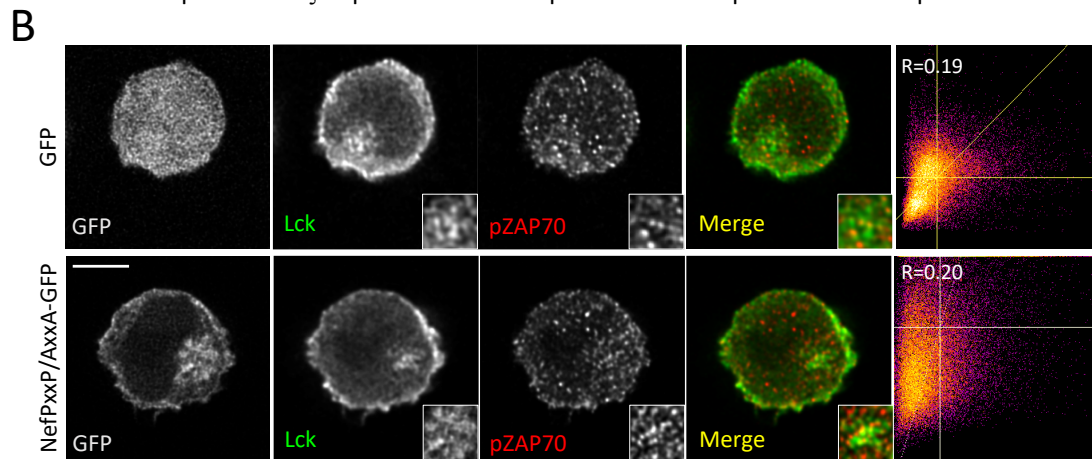
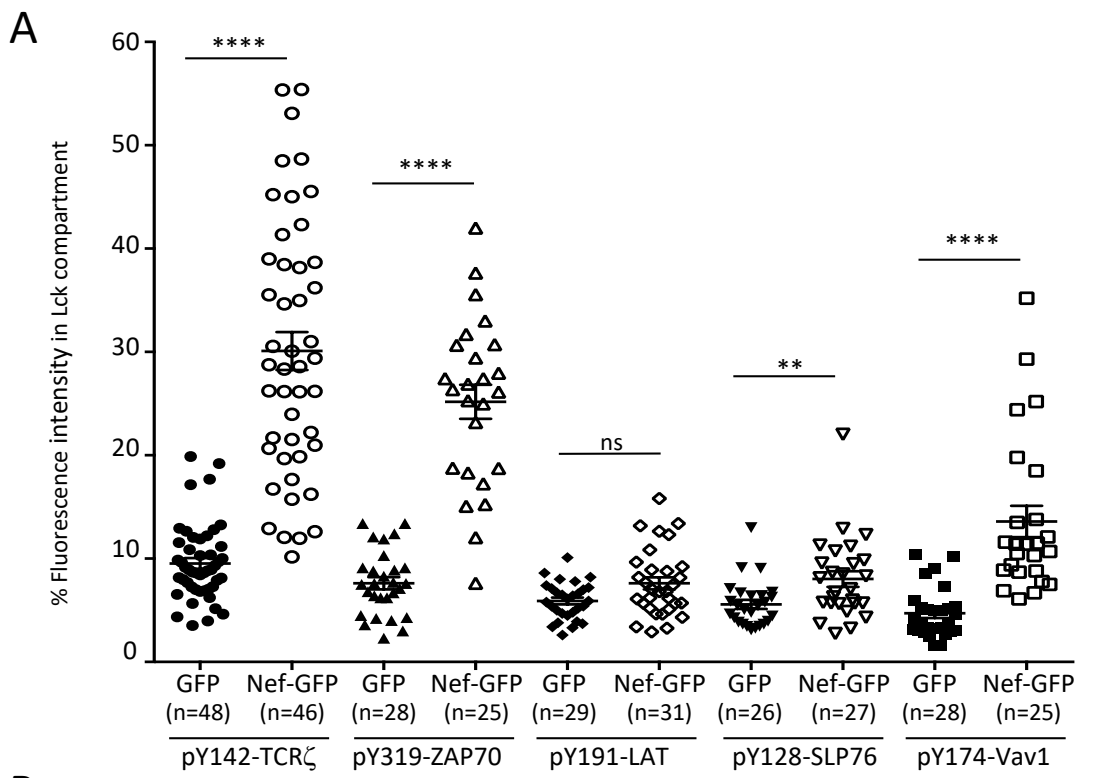


Figure 4

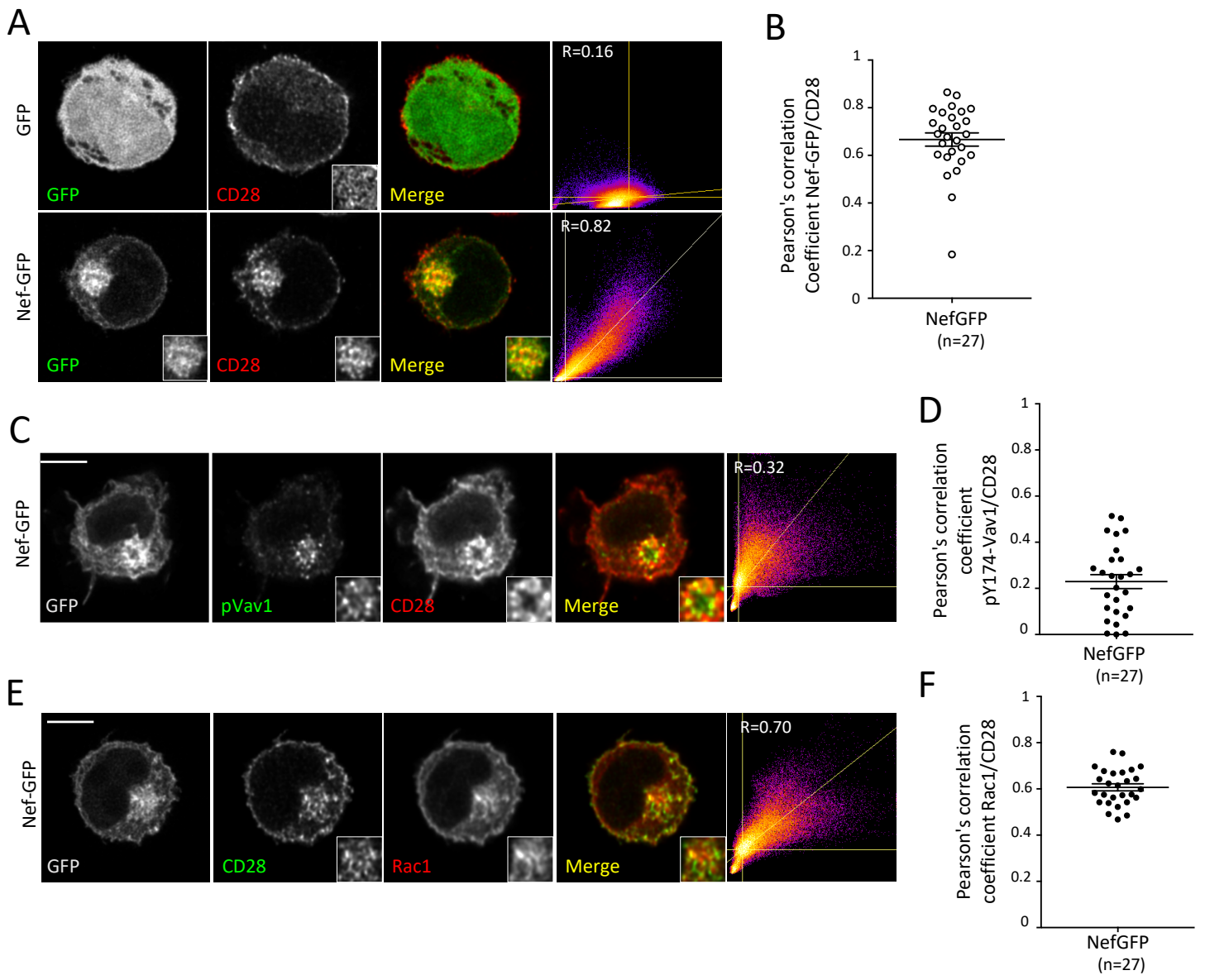


Figure 5

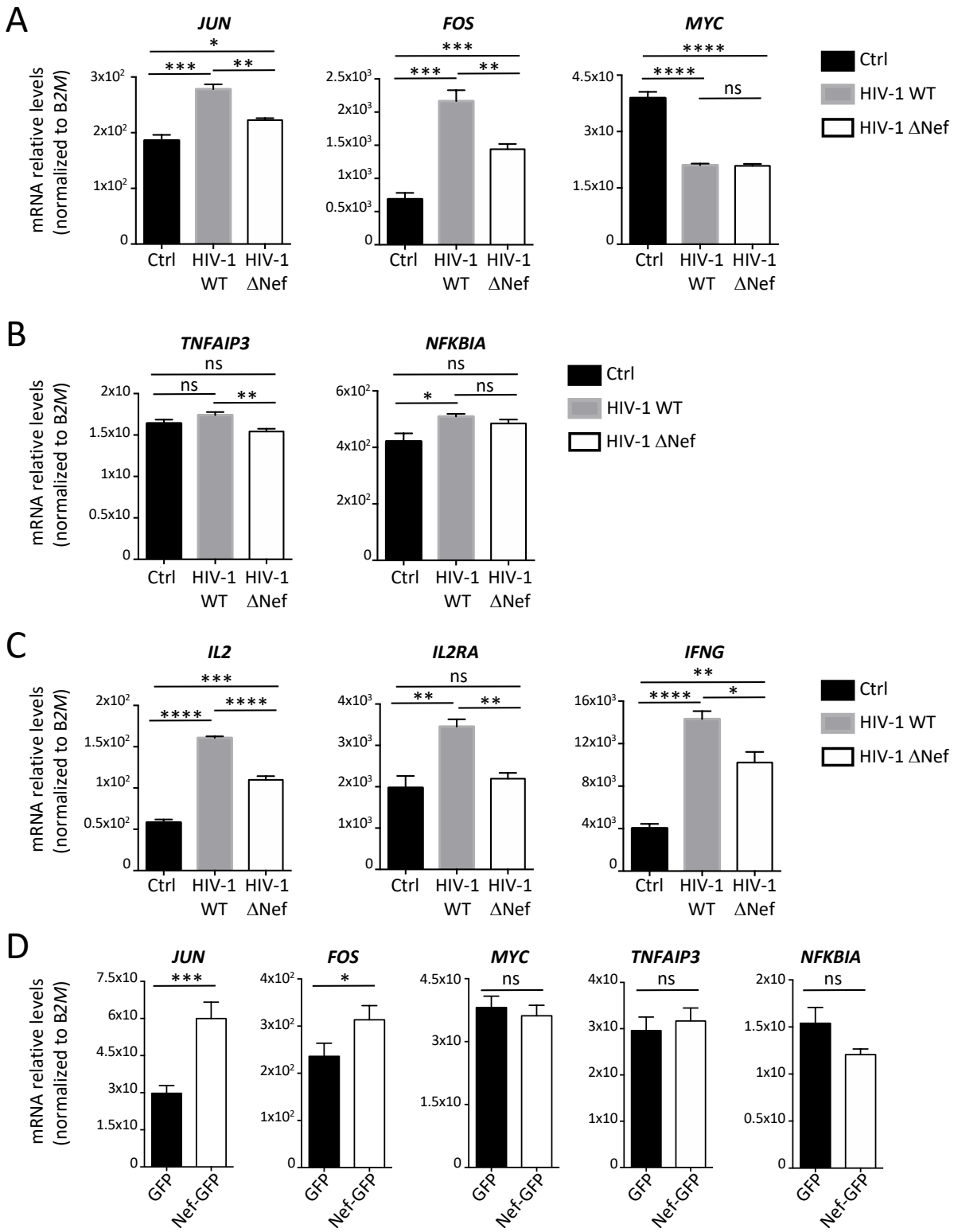


Figure 6

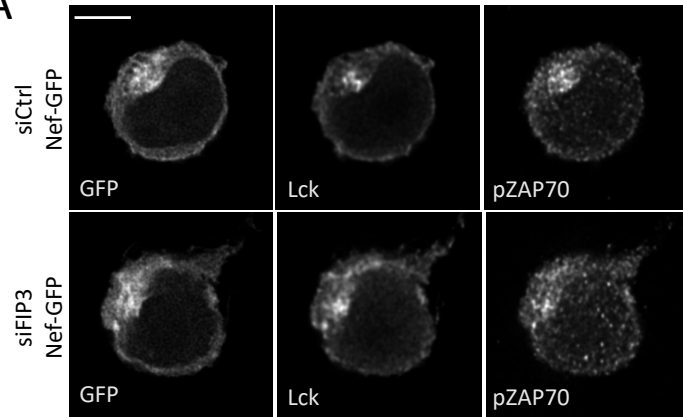
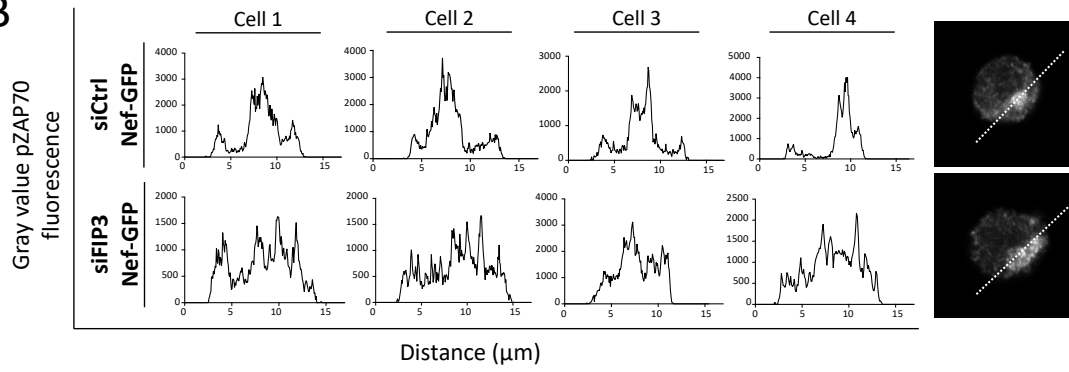
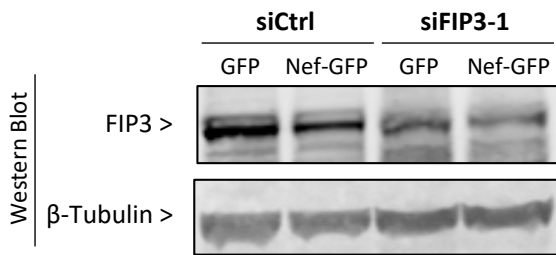
A**B****C**

Figure 7

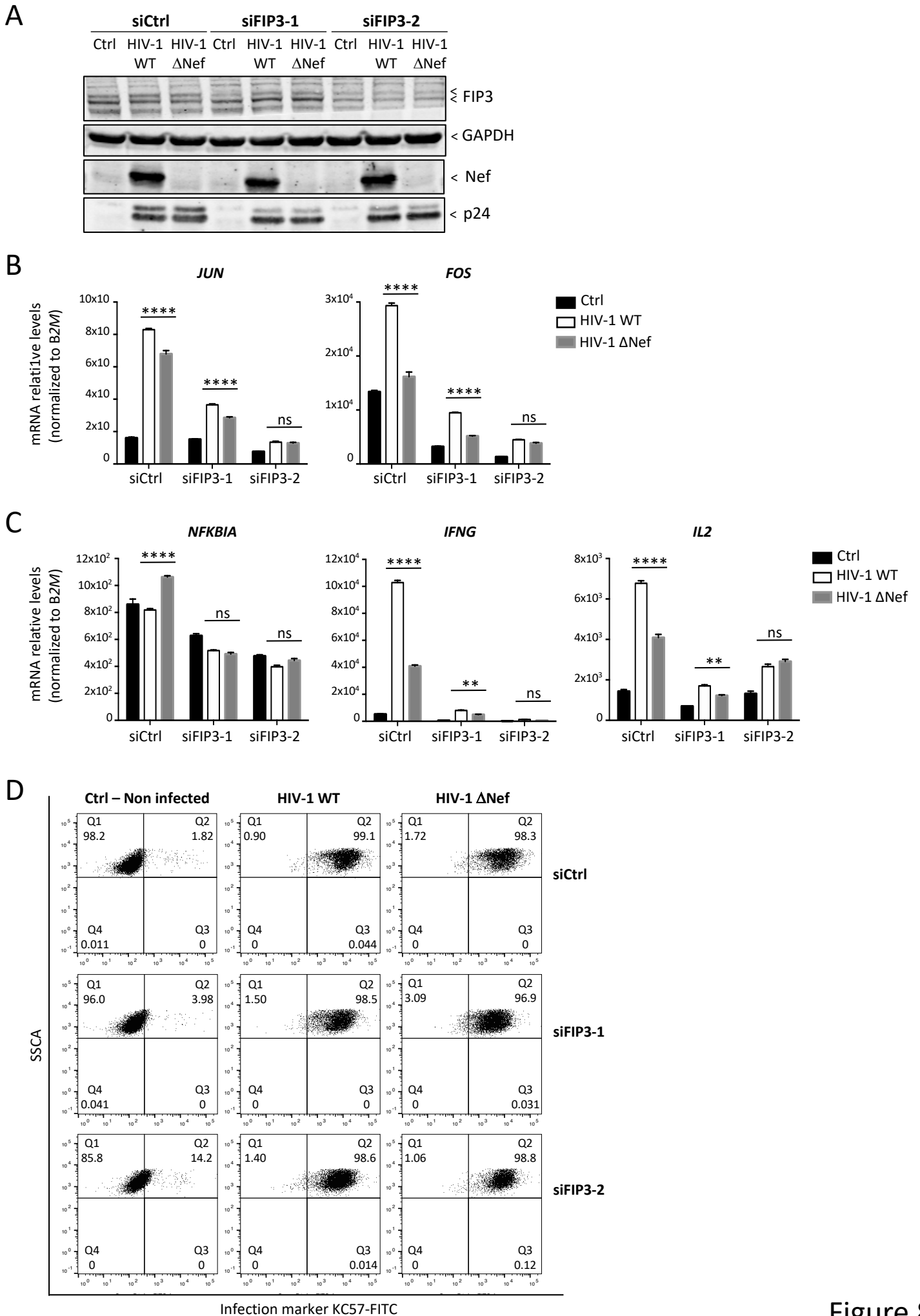


Figure 8

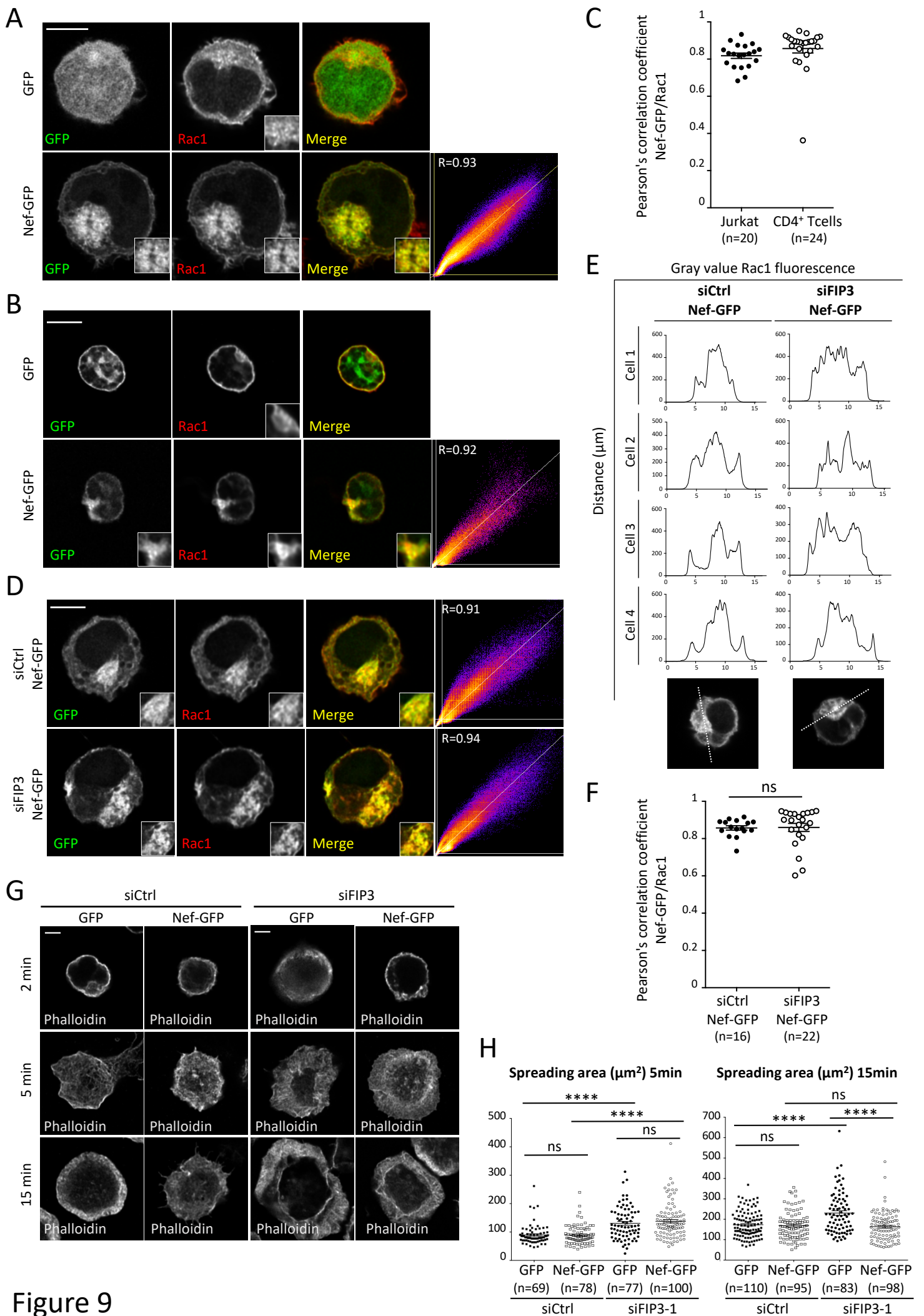
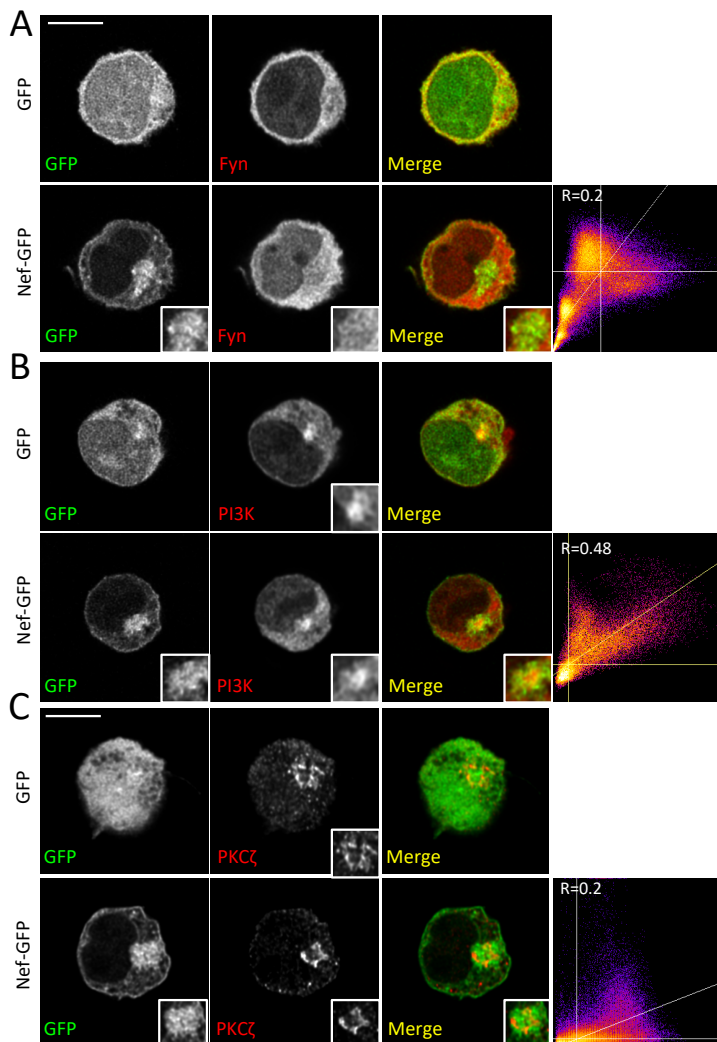


Figure 9



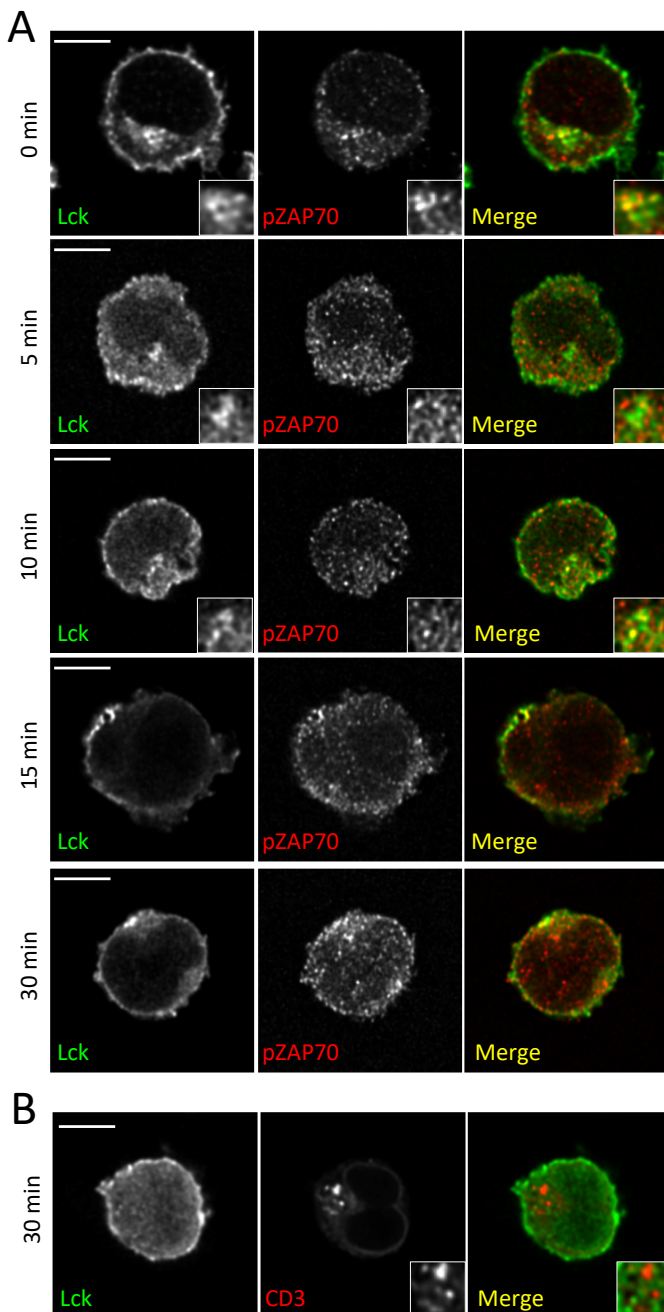
Protein	Localization
CD28, Lck, pY394-Lck, pY128-SLP76, pY142-TCRζ, pY319-ZAP70, pY174-Vav1, Rac1	Re-localized in the Nef-induced compartment
AKT, LAT, NEMO, pY783-PLCγ1, Vav1, ZAP70	Partially re-localized in the Nef-induced compartment
Bcl10, CARMA, Fyn, mTOR, NF-kappaB (p105 and p65 subunits), PI3K, PKCθ, PKCζ, pT202/Y204-Erk1/2, pY185-JNK, pY191-LAT, pT538-PKCθ, Rab11, TGN46	Non re-localized in the Nef-induced compartment

Supplementary Figure 1: Nef does not induce the relocalization of signaling effectors downstream of Lck, TCRζ, ZAP70 and Vav1

A-D: Localization of endogenous signaling proteins of the TCR and CD28 signaling pathways were analyzed in Jurkat T cells expressing GFP (top) or Nef-GFP (bottom) by immunofluorescence, using antibodies directed to the proteins or to specific phosphorylated amino acid residues (tyrosine or threonine) characterizing their signaling competent state.

A-C: Localization of endogenous Fyn (A), PI3K (B) and PKCζ (C) by immunofluorescence and confocal microscopy, here shown as examples of the numerous proteins analyzed and summarized in D. A z-stack of 0.2 μm-confocal optical sections was acquired for each cell. 3D confocal images were post-treated by deconvolution. A 0.4-μm-thick medial stack is shown. Bottom right corner of each image corresponds to a zoomed image of the pericentrosomal vesicular compartment of each cell. Analysis of colocalization between Nef-GFP and endogenous proteins was assessed by the Pearson's Correlation Coefficient (R). Bar, 5 μm.

D: List of the endogenous signaling proteins whose intracellular localization was analyzed during this study. Protein distributions assessed by visual observation of two observers were classified in 3 groups: re-localized in the Nef or the Nef-induced Lck pericentrosomal compartment (see figures in the main text), partially re-localized and no re-localized in those compartments. Localization of the proteins or their phosphorylated residues is depicted.



Supplementary Figure 2: CD3-CD28 stimulation does not mimic the Nef-induced Lck endosomal signaling compartment

A-B: Jurkat T cells transfected with GFP expression vector. Localization of endogenous Lck and phosphoTyr319-ZAP70 (**A**) or the internalized CD3 (**B**) after the indicated times of CD3-CD28 stimulation was assessed by immunofluorescence.

A z-stack of 0.2 μm -confocal optical sections was acquired for each cell. 3D confocal images were post-treated by deconvolution. A 0.4- μm -thick medial stack is shown. Bottom right corner images correspond to a zoomed image of the pericentrosomal vesicular compartment of each cell. Bar, 5 μm . Images representative of three experiments.

Primary antibodies/reagents - Specificity - Clone	Host-Isotype	Source	Dilution
Used in immunofluorescence			
AKT (pan) (40D4)	mouse IgG1	Cell Signaling	1:50
BCL10 (A48)	mouse IgG1	OriGene	7.3 µg/ml (1:100)
CARMA1 (CARD11)	rabbit	Abcam	33.3 µg/ml (1:30)
CD28 (B-T3)	mouse IgG2a	Abcam	10 µg/ml (1:100)
F-actin (Phalloidin - Texas Red)	Phallotoxin	Invitrogen	1:100
Fyn (FYN-01)	mouse IgG2b	Abcam	10 µg/ml (1:100)
HIV-1 p24 antiserum (Lot 060880)	rabbit	NIH AIDS Reagent Program	1:120
LAT	rabbit	Upstate Biotechnology	3.3 µg/ml (1:300)
Lck (3A5)	mouse IgG2b	Santa Cruz Biotechnology	2 µg/ml (1:100)
mTORC (7C10)	rabbit	Cell Signaling	1:400
NEMO	rabbit	Gift from Robert Weil	1:500
NF-κB (p105/50)	rabbit	Gift from Robert Weil	1:100
NF-κB (p65) (C-20)	rabbit	Santa Cruz Biotechnology	4 µg/ml (1:50)
Phospho-CD3ζ(Y142) (k25-407.69)	mouse IgG2a	Becton Dickinson	5 µg/ml (1:100)
Phospho-Erk1/2(T202/Y204) (D13.14.4E)	rabbit	Cell Signaling	1:200
Phospho-LAT(Y191)	rabbit	Cell Signaling	1:100
Phospho-PLCγ(Y783)	rabbit	Cell Signaling	1:100
Phospho-PKCθ(T538)	rabbit	Cell Signaling	1:100
Phospho-SAPK/JNK(T183/Y185) (G9)	mouse IgG1	Cell Signaling	1:400
Phospho-SLP76(Y128) (J141-668.36.58)	mouse IgG1	Becton Dickinson	2.5 µg/ml (1:200)
Phospho-Src family(Y416) (used to detect pY394-Lck)	rabbit	Cell Signaling	1:100
Phospho-ZAP70(Y319)/SYK(Y352) (65E4)	rabbit	Cell Signaling	1:100
Phospho-Vav1(Y174)	rabbit	Abcam	2.26 µg/ml (1:100)
PI3K (p85)	rabbit	Gift from S. Etienne-Manneville	1:100
PKCθ	mouse IgG2a	Becton Dickinson	2.5 µg/ml (1:100)
PKCζ (C-20)	rabbit	Santa Cruz Biotechnology	2 µg/ml (1:100)
Rab11 (47)	mouse IgG2a	Becton Dickinson	25 µg/ml (1:10)
Rac1 (102)	mouse IgG2b	Becton Dickinson	1.25 µg/ml (1:200)
TGN46	rabbit	Thermo Fisher	1.32 µg/ml (1:500)
ZAP70 (discontinued, ref 06-271)	rabbit	Upstate Biotechnology	1:100
Vav1 (M04) (3A11)	mouse IgG2a	Abnova (Interchim)	10 µg/ml (1:100)
Used for activation			
CD3ε (UCHT1)	mouse IgG1	BioLegend Inc.	10 µg/ml
CD28 (28.2)	mouse IgG1	Beckman Coulter	10 µg/ml
Used in flow cytometry			
HIV-1 proteins 55, 39, 33 & 24kD of core antigen (KC57-FITC/FH190-1-1)	mouse IgG1	Beckman Coulter	1:200
Used in western blot			
β-Tubullin (KMX-1)	mouse IgG2b	Millipore	1 µg/ml (1:1000)
Rab11-FIP3	rabbit	www.antibodies-online.com	2.4 µg/ml (1:500)
GAPDH (0411)	mouse IgG1	Santa Cruz Biotechnology	0.1 µg/ml (1:2000)
HIV-1 Nef (6.2) (Lot V9R01009A-004)	mouse IgG1	NIH AIDS Reagent Program	1:500
HIV-1 p24 (AG3.0) (Lot 6 120227)	mouse IgG1	NIH AIDS Reagent Program	1:500
Secondary Antibodies	Conjugated fluorophore	Source	Dilution
Used in immunofluorescence			
Goat anti-Fluorescein/Oregon Green	Alexa Fluor 488	Molecular Probes	10 µg/ml (1:100)
Goat anti-mouse IgG1	Cy3	Jackson ImmunoResearch	15 µg/ml (1:100)
Goat anti-mouse IgG1	Cy5	Jackson ImmunoResearch	7.5 µg/ml (1:200)
Goat anti-mouse IgG2a	Cy3	Jackson ImmunoResearch	7 µg/ml (1:200)
Goat anti-mouse IgG2b	Alexa Fluor 647	Jackson ImmunoResearch	15 µg/ml (1:100)
Goat anti-mouse IgG2b	Cy3	Jackson ImmunoResearch	7.5 µg/ml (1:200)
Goat anti-rabbit	Cy3	Jackson ImmunoResearch	7.5 µg/ml (1:200)
Goat anti-rabbit	FITC	Jackson ImmunoResearch	7.5 µg/ml (1:200)
Used in western blot			
Goat anti-mouse IgG	DyLight800	Thermo Scientific	100 ng/ml (1:10000)
Goat anti-rabbit IgG	DyLight800	Thermo Scientific	62.5 ng/ml (1:8000)

Supplementary Table 1. Primary and secondary antibodies/reagents used for activation, immunofluorescence, flow cytometry and western blot

Gene	Forward	Reverse
<i>B2M</i>	5'-TGACTTTGTCACAGCCCAAGATA-3'	5'-AATGCGGCATCTTCAAACCT-3'
<i>CXCL8</i>	5'-GCCTTCCTGATTTCTGCAGC-3'	5'-TTGGGGTGGAAAGTTTGGA-3'
<i>FOS</i>	5'-CGAGCGCAGAGCATTGG-3'	5'-CCTTCGGATTCTCCTTTTCTCTT-3'
<i>IL2</i>	5'-ACCTCAACTCCTGCCACAAT-3'	5'-TGAGCATCCTGGTGAGTTTG-3'
<i>IL2RA</i> (<i>CD25</i>)	5'-ATCAGTGCGTCCAGGGATAC-3'	5'-GACGAGGCAGGAAGTCTCAC-3'
<i>IFNG</i>	5'-GAAACGAGATGACTTCGAAAAGCTGAC-3'	5'-CTGCTGGCGACAGTTCAGCCAT-3'
<i>JUN</i>	5'-TGACTGCAAAGATGGAAACG-3'	5'-CAGGGTCATGCTCTGTTTCA-3'
<i>MYC</i>	5'-GAGGCTATTCTGCCCATTTG-3'	5'-CACCGAGTCGTAGTCGAGGT-3'
<i>NFKBIA</i>	5'-GAGCTTTTGGTGTCTTGGG-3'	5'-CATCAGCCCCACACTTCAAC-3'
<i>TNFAIP3</i>	5'-TAGAAATCCCCGTCCAAGGC-3'	5'-AGCTTCATCCAACCTTTCGGG-3'

Supplementary Table 2. Primer sequences